



UvA-DARE (Digital Academic Repository)

Search for lepton flavor violation in $e p$ collisions at 300-GeV center-of-mass energy

Derrick (et al.), M.; Botje, M.A.J.; Chlebana, F.S.; Engelen, J.J.; de Kamps, M.; Kooijman, P.M.; Kruse, A.; van Sighem, A.I.; Tiecke, H.G.J.M.; Verkerke, W.; Vossebeld, J.H.; Vreeswijk, M.; Wiggers, L.W.; de Wolf, E.; van Woudenberg, R.

Published in:

Zeitschrift für Physik. C, Particles and Fields

DOI:

[10.1007/s002880050352](https://doi.org/10.1007/s002880050352)

[Link to publication](#)

Citation for published version (APA):

Derrick (et al.), M., Botje, M. A. J., Chlebana, F. S., Engelen, J. J., de Kamps, M., Kooijman, P. M., ... van Woudenberg, R. (1997). Search for lepton flavor violation in $e p$ collisions at 300-GeV center-of-mass energy. *Zeitschrift für Physik. C, Particles and Fields*, 73, 613. <https://doi.org/10.1007/s002880050352>

General rights

It is not permitted to download or to forward/distribute the text or part of it without the consent of the author(s) and/or copyright holder(s), other than for strictly personal, individual use, unless the work is under an open content license (like Creative Commons).

Disclaimer/Complaints regulations

If you believe that digital publication of certain material infringes any of your rights or (privacy) interests, please let the Library know, stating your reasons. In case of a legitimate complaint, the Library will make the material inaccessible and/or remove it from the website. Please Ask the Library: <https://uba.uva.nl/en/contact>, or a letter to: Library of the University of Amsterdam, Secretariat, Singel 425, 1012 WP Amsterdam, The Netherlands. You will be contacted as soon as possible.

Search for lepton flavor violation in ep collisions at 300 GeV center of mass energy

ZEUS Collaboration

M. Derrick, D. Krakauer, S. Magill, D. Mikunas, B. Musgrave, J.R. Okrasinski, J. Repond, R. Stanek, R.L. Talaga, H. Zhang

Argonne National Laboratory, Argonne, IL 60439, USA ^p

M.C.K. Mattingly

Andrews University, Berrien Springs, MI, USA

F. Anselmo, P. Antonioli, G. Bari, M. Basile, L. Bellagamba, D. Boscherini, A. Bruni, G. Bruni, P. Bruni, G. Cara Romeo, G. Castellini¹, L. Cifarelli², F. Cindolo, A. Contin, M. Corradi, I. Gialas, P. Giusti, G. Iacobucci, G. Laurenti, G. Levi, A. Margotti, T. Massam, R. Nania, F. Palmonari, A. Pesci, A. Polini, G. Sartorelli, Y. Zamora Garcia³, A. Zichichi
University and INFN Bologna, I-40126 Bologna, Italy ^f

C. Amelung, A. Bornheim, J. Crittenden, R. Deffner, M. Eckert, L. Feld, A. Frey⁴, M. Geerts⁵, M. Grothe, H. Hartmann, K. Heinloth, L. Heinz, E. Hilger, H.-P. Jakob, U.F. Katz, S. Mengel⁶, E. Paul, M. Pfeiffer, Ch. Rembser, D. Schramm⁷, J. Stamm, R. Wedemeyer

Physikalisches Institut der Universität Bonn, D-53115 Bonn, Germany ^c

S. Campbell-Robson, A. Cassidy, W.N. Cottingham, N. Dyce, B. Foster, S. George, M.E. Hayes, G.P. Heath, H.F. Heath, D. Piccioni, D.G. Roff, R.J. Tapper, R. Yoshida

H.H. Wills Physics Laboratory, University of Bristol, Bristol B58 1TL, U.K. ^o

M. Arneodo⁸, R. Ayad, M. Capua, A. Garfagnini, L. Iannotti, M. Schioppa, G. Susinno

Calabria University, Physics Dept. and INFN, Cosenza, Italy ^f

A. Caldwell⁹, N. Cartiglia, Z. Jing, W. Liu, J.A. Parsons, S. Ritz¹⁰, F. Sciulli, P.B. Straub, L. Wai¹¹, S. Yang¹², Q. Zhu

Columbia University, Nevis Labs., Irvington on Hudson, NY 10533, USA ^q

P. Borzemeski, J. Chwastowski, A. Eskreys, Z. Jakubowski, M.B. Przybycień, M. Zachara, L. Zawiejski

Inst. of Nuclear Physics, PL-30055 Cracow, Poland ^j

L. Adamczyk, B. Bednarek, K. Jeleń, D. Kisielewska, T. Kowalski, M. Przybycień, E. Rulikowska-Zarebska, L. Suszycki, J. Zając

Faculty of Physics and Nuclear Techniques, Academy of Mining and Metallurgy, PL-30055 Cracow, Poland ^j

Z. Duliński, A. Kotański

Jagellonian Univ., Dept. of Physics, PL-30059 Cracow, Poland ^k

G. Abbiendi¹³, L.A.T. Bauerdick, U. Behrens, H. Beier, J.K. Bienlein, G. Cases, O. Deppe, K. Desler, G. Drews, M. Flasiński¹⁴, D.J. Gilkinson, C. Glasman, P. Göttlicher, J. Große-Knetter, T. Haas, W. Hain, D. Hasell, H. Heßling, Y. Iga, K.F. Johnson¹⁵, P. Joos, M. Kasemann, R. Klanner, W. Koch, U. Kötz, H. Kowalski, J. Labs, A. Ladage, B. Lühr, M. Löwe, D. Lüke, J. Mainusch¹⁶, O. Mańczak, J. Milewski, T. Monteiro¹⁷, J.S.T. Ng, D. Notz, K. Ohrenberg, K. Piotrkowski, M. Roco, M. Rohde, J. Roldán, U. Schneekloth, W. Schulz, F. Selonke, B. Sorrow, E. Tassi, T. Voß, D. Westphal, G. Wolf, U. Wollmer, C. Youngman, W. Zeuner

Deutsches Elektronen-Synchrotron DESY, D-22603 Hamburg, Germany

H.J. Grabosch, S.M. Mari¹⁸, A. Meyer, S. Schlenstedt

DESY-IfH Zeuthen, D-15738 Zeuthen, Germany

G. Barbagli, E. Gallo, P. Pelfer

University and INFN, Florence, Italy ^f

G. Maccarrone, S. De Pasquale, L. Votano

INFN, Laboratori Nazionali di Frascati, I-00044 Frascati, Italy ^f

A. Bamberger, S. Eisenhardt, T. Trefzger¹⁹, S. Wölfle

Fakultät für Physik der Universität Freiburg i.Br., D-79104 Freiburg i.Br., Germany ^c

J.T. Bromley, N.H. Brook, P.J. Bussey, A.T. Doyle, D.H. Saxon, L.E. Sinclair, E. Strickland, M.L. Utley, R. Waugh, A.S. Wilson

Dept. of Physics and Astronomy, University of Glasgow, Glasgow G12 8QQ, U.K. ^o

A. Dannemann²⁰, U. Holm, D. Horstmann, R. Sinkus²¹, K. Wick

Hamburg University, I. Institute of Exp. Physics, D-22761 Hamburg, Germany ^c

B.D. Burow²², L. Hagge¹⁶, E. Lohrmann, G. Poelz, W. Schott, F. Zetsche

Hamburg University, II. Institute of Exp. Physics, D-22761 Hamburg, Germany ^c

T.C. Bacon, N. Brümmer, I. Butterworth, V.L. Harris, G. Howell, B.H.Y. Hung, L. Lamberti²³, K.R. Long, D.B. Miller, N. Pavel, A. Priniyas²⁴, J.K. Sedgbeer, D. Sideris, A.F. Whitfield

Imperial College London, High Energy Nuclear Physics Group, London SW7 2BZ, U.K. ^o

U. Mallik, M.Z. Wang, S.M. Wang, J.T. Wu

University of Iowa, Physics and Astronomy Dept., Iowa City, IA 52242, USA ^p

P. Cloth, D. Filges

Forschungszentrum Jülich, Institut für Kernphysik, D-52405 Jülich, Germany

S.H. An, G.H. Cho, B.J. Ko, S.B. Lee, S.W. Nam, H.S. Park, S.K. Park

Korea University, Seoul 136-701, Korea ^h

S. Kartik, H.-J. Kim, R.R. McNeil, W. Metcalf, V.K. Nadendla

Louisiana State University, Dept. of Physics and Astronomy, Baton Rouge, LA 70803-4001, USA ^p

F. Barreiro, J.P. Fernandez, R. Graciani, J.M. Hernández, L. Hervás, L. Labarga, M. Martinez, J. del Peso, J. Puga, J. Terron, J.F. de Trocóniz

Univer. Autónoma Madrid, Depto de Física Teórica, E-28049 Madrid, Spain ⁿ

F. Corriveau, D.S. Hanna, J. Hartmann, L.W. Hung, J.N. Lim, C.G. Matthews²⁵, W.N. Murray, A. Ochs, P.M. Patel, M. Riveline, D.G. Stairs, M. St-Laurent, R. Ullmann, G. Zacek²⁵

McGill University, Dept. of Physics, Montréal, PQ H3A 2T8, Canada ^{a, b}

T. Tsurugai

Meiji Gakuin University, Faculty of General Education, Yokohama 244, Japan

V. Bashkurov, B.A. Dolgoshein, A. Stifutkin

Moscow Engineering Physics Institute, RU-115 409 Moscow, Russia ^l

G.L. Bashindzhagyan²⁶, P.F. Ermolov, L.K. Gladilin, Yu.A. Golubkov, V.D. Kobrin, I.A. Korzhavina, V.A. Kuzmin, O.Yu. Lukina, A.S. Proskuryakov, A.A. Savin, L.M. Shcheglova, A.N. Solomin, N.P. Zotov

Moscow State University, Institute of Nuclear Physics, RU-119 899 Moscow, Russia ^m

M. Botje, F. Chlebana, J. Engelen, M. de Kamps, P. Kooijman, A. Kruse, A. van Sighem, H. Tiecke, W. Verkerke, J. Vossebeld, M. Vreeswijk, L. Wiggers, E. de Wolf, R. van Woudenberg²⁷

NIKHEF and University of Amsterdam, NL-1009 DB Amsterdam, Netherlands ⁱ

D. Acosta, B. Bylsma, L.S. Durkin, J. Gilmore, C.M. Ginsburg, C.L. Kim, C. Li, T.Y. Ling, P. Nylander, I.H. Park, T.A. Romanowski²⁸

Ohio State University, Physics Department, Columbus, OH 43210-1106, USA ^p

D.S. Bailey, R.J. Cashmore²⁹, A.M. Cooper-Sarkar, R.C.E. Devenish, N. Harnew, M. Lancaster³⁰,

L. Lindemann, J.D. McFall, C. Nath, V.A. Noyes²⁴, A. Quadt, J.R. Tickner, H. Uijterwaal, R. Walczak, D.S. Waters, F.F. Wilson, T. Yip

Department of Physics, University of Oxford, Oxford, U.K. ^o

A. Bertolin, R. Brugnera, R. Carlin, F. Dal Corso, M. De Giorgi, U. Dosselli, S. Limentani, M. Morandin, M. Posocco, L. Stanco, R. Stroili, C. Voci, F. Zuin

Dipartimento di Fisica dell' Università and INFN, I-35131 Padova, Italy ^f

J. Bulmahn, R.G. Feild³¹, B.Y. Oh, J.J. Whitmore

Pennsylvania State University, Dept. of Physics, University Park, PA 16802, USA ^q

G. D'Agostini, G. Marini, A. Nigro

Dipartimento di Fisica, Univ. 'La Sapienza' and INFN, I-00185 Rome, Italy ^f

J.C. Hart, N.A. McCubbin, T.P. Shah

Rutherford Appleton Laboratory, Chilton, Didcot OX11 0QX, U.K. ^o

E. Barberis, T. Dubbs, C. Heusch, M. Van Hook, W. Lockman, J.T. Rahn, H.F.-W. Sadrozinski, A. Seiden, D.C. Williams
University of California, Santa Cruz, CA 93106, USA ^p

J. Biltzinger, R.J. Seifert, O. Schwarzer, A.H. Walenta

Fachbereich Physik der Universität-Gesamthochschule Siegen, D-57012 Siegen, Germany ^c

H. Abramowicz, G. Briskin, S. Dagan³², T. Doeker³², A. Levy²⁶

Raymond and Beverly Sackler Faculty of Exact Sciences, School of Physics, Tel-Aviv University, Tel-Aviv 69978, Israel ^e

J.I. Fleck³³, M. Inuzuka, T. Ishii, M. Kuze, S. Mine, M. Nakao, I. Suzuki, K. Tokushuku,
K. Umemori, S. Yamada, Y. Yamazaki

Institute for Nuclear Study, University of Tokyo, Tokyo 113, Japan ^g

M. Chiba, R. Hamatsu, T. Hirose, K. Homma, S. Kitamura³⁴, T. Matsushita, K. Yamauchi

Tokyo Metropolitan University, Dept. of Physics, Tokyo 192-03, Japan ^g

R. Cirio, M. Costa, M.I. Ferrero, S. Maselli, C. Peroni, R. Sacchi, A. Solano, A. Staiano

Universita di Torino, Dipartimento di Fisica Sperimentale and INFN, I-10129 Torino, Italy ^f

M. Dardo

II Faculty of Sciences, Torino University and INFN - Alessandria, Italy ^f

D.C. Bailey, F. Benard, M. Brkic, C.-P. Fagerstroem, G.F. Hartner, K.K. Joo, G.M. Levman, J.F. Martin, R.S. Orr,
S. Polenz, C.R. Sampson, D. Simmons, R.J. Teuscher

University of Toronto, Dept. of Physics, Toronto, ON M5S 1A7, Canada ^a

J.M. Butterworth, C.D. Catterall, T.W. Jones, P.B. Kaziewicz, J.B. Lane, R.L. Saunders, J. Shulman, M.R. Sutton

University College London, Physics and Astronomy Dept., London WC1E 6BT, U.K. ^o

B. Lu, L.W. Mo

Virginia Polytechnic Inst. and State University, Physics Dept., Blacksburg, VA 24061, USA ^q

W. Bogusz, J. Ciborowski, J. Gajewski, G. Grzelak³⁵, M. Kasprzak, M. Krzyżanowski,

K. Muchorowski³⁶, R.J. Nowak, J.M. Pawlak, T. Tymieniecka, A.K. Wróblewski, J.A. Zakrzewski, A.F. Żarnecki
Warsaw University, Institute of Experimental Physics, PL-00681 Warsaw, Poland ^j

M. Adamus

Institute for Nuclear Studies, PL-00681 Warsaw, Poland ^j

C. Coldewey, Y. Eisenberg³², D. Hochman, U. Karshon³², D. Revel³², D. Zer-Zion

Weizmann Institute, Nuclear Physics Dept., Rehovot 76100, Israel ^d

W.F. Badgett, J. Breitweg, D. Chapin, R. Cross, S. Dasu, C. Foudas, R.J. Loveless, S. Mattingly, D.D. Reeder, S. Silverstein,
W.H. Smith, A. Vaiciulis, M. Wodarczyk

University of Wisconsin, Dept. of Physics, Madison, WI 53706, USA ^p

S. Bhadra, M.L. Cardy³⁷, W.R. Frisken, M. Khakzad, W.B. Schmidke

York University, Dept. of Physics, North York, Toronto ON M3J 1P3, Canada ^a

Received: 16 August 1996 / Revised version: 29 October 1996

¹ also at IROE Florence, Italy
² now at Univ. of Salerno and INFN Napoli, Italy
³ supported by Worldlab, Lausanne, Switzerland
⁴ now at Univ. of California, Santa Cruz
⁵ now a self-employed consultant
⁶ now at VDI-Technologiezentrum Düsseldorf
⁷ now at Commasoft, Bonn
⁸ also at University of Torino and Alexander von Humboldt Fellow
⁹ Alexander von Humboldt Fellow
¹⁰ Alfred P. Sloan Foundation Fellow
¹¹ now at University of Washington, Seattle
¹² now at California Institute of Technology, Los Angeles
¹³ supported by an EC fellowship number ERBFMBICT 950172
¹⁴ now at Inst. of Computer Science, Jagellonian Univ., Cracow

¹⁵ visitor from Florida State University
¹⁶ now at DESY Computer Center
¹⁷ supported by European Community Program PRAXIS XXI
¹⁸ present address: Dipartimento di Fisica, Univ. "La Sapienza", Rome
¹⁹ now at ATLAS Collaboration, Univ. of Munich
²⁰ now at Star Division Entwicklungs- und Vertriebs-GmbH, Hamburg
²¹ now at Philips Medizin Systeme, Hamburg
²² also supported by NSERC, Canada
²³ supported by an EC fellowship
²⁴ PPARC Post-doctoral Fellow
²⁵ now at Park Medical Systems Inc., Lachine, Canada
²⁶ partially supported by DESY
²⁷ now at Philips Natlab, Eindhoven, NL
²⁸ now at Department of Energy, Washington

Abstract. Using the ZEUS detector at the HERA electron-proton collider, we have searched for lepton flavor violation in ep collisions at a center-of-mass energy (\sqrt{s}) of 300 GeV. Events of the type $e + p \rightarrow \ell + X$ with a final-state lepton of high transverse momentum, $\ell = \mu$ or τ , were sought. No evidence was found for lepton flavor violation in the combined 1993 and 1994 data samples, for which the integrated luminosities were 0.84 pb^{-1} for e^-p collisions and 2.94 pb^{-1} for e^+p collisions. Limits on coupling *vs.* mass are provided for leptoquarks and R -parity violating squarks. For flavor violating couplings of electromagnetic strength, we set 95% confidence level lower limits on leptoquark masses between 207 GeV and 272 GeV, depending on the leptoquark species and final-state lepton. For leptoquark masses larger than 300 GeV, limits on flavor-changing couplings are determined, many of which supersede prior limits from rare decay processes.

²⁹ also at University of Hamburg, Alexander von Humboldt Research Award

³⁰ now at Lawrence Berkeley Laboratory, Berkeley

³¹ now at Yale University, New Haven, CT

³² supported by a MINERVA Fellowship

³³ supported by the Japan Society for the Promotion of Science (JSPS)

³⁴ present address: Tokyo Metropolitan College of Allied Medical Sciences, Tokyo 116, Japan

³⁵ supported by the Polish State Committee for Scientific Research, grant No. 2P03B09308

³⁶ supported by the Polish State Committee for Scientific Research, grant No. 2P03B09208

³⁷ now at TECMAR Incorporated, Toronto

^a supported by the Natural Sciences and Engineering Research Council of Canada (NSERC)

^b supported by the FCAR of Québec, Canada

^c supported by the German Federal Ministry for Education and Science, Research and Technology (BMBF), under contract numbers 057BN19P, 057FR19P, 057HH19P, 057HH29P, 057SI75I

^d supported by the MINERVA Gesellschaft für Forschung GmbH, the Israel Academy of Science and the U.S.-Israel Binational Science Foundation

^e supported by the German Israeli Foundation, and by the Israel Academy of Science

^f supported by the Italian National Institute for Nuclear Physics (INFN)

^g supported by the Japanese Ministry of Education, Science and Culture (the Monbusho) and its grants for Scientific Research

^h supported by the Korean Ministry of Education and Korea Science and Engineering Foundation

ⁱ supported by the Netherlands Foundation for Research on Matter (FOM)

^j supported by the Polish State Committee for Scientific Research, grants No. 115/E-343/SPUB/P03/109/95, 2P03B 244 08p02, p03, p04 and p05, and the Foundation for Polish-German Collaboration (proj. No. 506/92)

^k supported by the Polish State Committee for Scientific Research (grant No. 2 P03B 083 08) and Foundation for Polish-German Collaboration

^l partially supported by the German Federal Ministry for Education and Science, Research and Technology (BMBF)

^m supported by the German Federal Ministry for Education and Science, Research and Technology (BMBF), and the Fund of Fundamental Research of Russian Ministry of Science and Education and by INTAS-Grant No. 93-63

ⁿ supported by the Spanish Ministry of Education and Science through funds provided by CICYT

^o supported by the Particle Physics and Astronomy Research Council

^p supported by the US Department of Energy

^q supported by the US National Science Foundation

1 Introduction

Lepton flavor is conserved in all interactions of the Standard Model (SM); discovery of lepton-flavor violation (LFV) in any form would be evidence for physics beyond our principal particle physics paradigm. Many searches for specific reactions which violate lepton flavor have been performed. The most sensitive include searches for $\mu + N \rightarrow e + N$ using very low-energy muons [1], for the forbidden muon decay $\mu \rightarrow e\gamma$ [2], and for forbidden leptonic kaon decays [3]. The limits from these processes are sensitive to $e \leftrightarrow \mu$ flavor change, but not to $e \leftrightarrow \tau$. Also, each of these processes involves specific quark flavors: in the first case, only first generation quarks participate; in the second case, for mechanisms which involve virtual quarks, the same quark flavor must couple to both e and μ ; in the last case, strange quarks must be involved. Since lepton flavor change could involve the τ -lepton or could be accompanied by quark flavor change, there may be LFV reactions which would be invisible to these very sensitive experiments. Hence, we have no *a priori* reason to assume that flavor violation, should it exist, will be visible through these specific reactions. Therefore, though less sensitive in an absolute sense, other manifestations of flavor violation, like forbidden leptonic decays of B - and D -mesons and of τ -leptons, are being investigated [4].

We report here a search for LFV carried out by the ZEUS collaboration at the HERA ep collider where we have sought instances of the reaction

$$e + p \rightarrow \ell + X, \quad (1)$$

where ℓ represents an isolated final-state μ or τ with large transverse momentum and X represents the hadronic final state. Processes with such topologies can be found in ZEUS with good efficiency and with little background. It should be emphasized that any reaction of the type (1) in which a final-state high-energy μ or τ replaces the incident electron¹ would be direct evidence for physics beyond the Standard Model, independent of the underlying mechanism. Furthermore, this reaction should occur at some level for a wide range of possible LFV mechanisms. LFV mechanisms which also involve a quark flavor change, or which are stronger for heavier quarks [5] may be seen more readily at HERA, where the sensitivity is largely independent of quark flavor², than in low-energy experiments.

The lepton-flavor violating reaction (1) could occur via s -, u -, or t -channel exchanges as shown in Fig. 1. For the s - and u -channel processes the exchanged particle has the quantum numbers of a leptoquark (or an R -parity violating squark). The cross sections depend on the leptoquark species and mass, and on the couplings, λ_{eq_1} and $\lambda_{\ell q_2}$ shown in Fig. 1. For the case of t -channel exchange, the process would be mediated by a flavor-changing neutral boson.

For definiteness, we will describe reaction (1) with leptoquarks as the carrier of the LFV force, treating separately the

¹ In the following, "electron" is generically used to denote both electrons and positrons

² Though the threshold for top (t) quark production is below the HERA center-of-mass energy, with present luminosities t production would only be observable if the couplings were very large. Therefore, we choose not to report on LFV couplings involving top in this paper

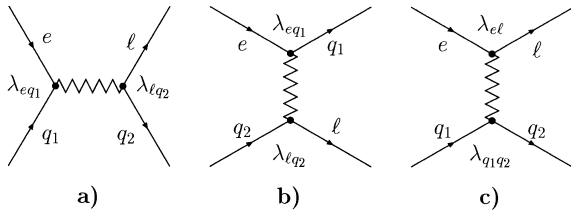


Fig. 1. The (a) s -, (b) u -, and (c) t -channel Feynman diagrams for LFV. For the s -channel and u -channel diagrams, we denote the couplings as $\lambda_{\ell q}$, where the indices refer to the lepton and quark flavors

cases of direct leptoquark production and the virtual effects of leptoquarks with masses above 300 GeV. The similarity of production formulae between R -parity-violating squarks and certain leptoquarks permits us to relate the couplings implied by the two mechanisms for a specified cross section. Results on flavor violation induced by leptogluons or by flavor-changing neutral bosons as well as details of the technique used in this analysis are also available [6]. The H1 collaboration [7] has also searched for direct production of leptoquarks with flavor-violating couplings using similar methods.

This analysis is based on an integrated luminosity of 0.84 pb^{-1} (2.94 pb^{-1}) of e^-p (e^+p) data taken during the 1993 and 1994 running periods. Beam energies at HERA were 26.7 GeV (27.5 GeV) for the electron beam in 1993 (1994) and 820 GeV for the proton beam. The resulting center-of-mass energy of 296 GeV (300 GeV) is an order of magnitude higher than for fixed-target lepton-nucleon scattering experiments.

2 Scenarios of lepton flavor violation

2.1 Leptoquarks

A leptoquark (LQ) is a hypothetical color triplet boson with fractional electric charge, and non-zero lepton and baryon numbers. Such particles are often invoked in extensions of the SM, *e.g.* in grand unified theories and technicolor models [8]. It is possible, indeed desirable in some models, that an LQ couple to multiple lepton and/or quark flavors, thereby providing a mechanism for flavor violation.

The simplest models involving a flavor-violating leptoquark would be characterized by three parameters: the leptoquark mass, and the coupling at each lepton-quark-leptoquark vertex. In order to avoid models which would involve additional parameters, we have assumed the following four points:

- 1) the LQ has $SU(3)_C \times SU(2)_L \times U(1)_Y$ invariant couplings,
- 2) the LQ has either left- or right-handed couplings, but not both (*i.e.* $\lambda_L \lambda_R = 0$),
- 3) the members of each weak-isospin multiplet are degenerate in mass,
- 4) one LQ species dominates the production process.

There are fourteen species of leptoquarks which satisfy these conditions [9]. For fermion number $F \equiv L + 3B$ (L and B denote lepton and baryon number) equal to zero, the species

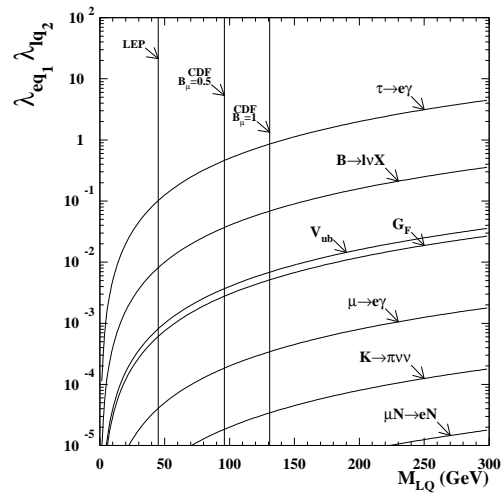


Fig. 2. Existing 95% CL limits [10] on the product of the couplings $\lambda_{eq_1} \lambda_{\ell q_2}$ vs. leptoquark mass M_{LQ} for a S_0^L leptoquark mediating $e \leftrightarrow \mu$ and $e \leftrightarrow \tau$ transitions accompanied by various quark flavor changes. Each limit curve excludes the region above it. The vertical lines indicate lower limits of allowed leptoquark mass from LEP [11] and the Tevatron [12]. The Tevatron limits apply to any scalar leptoquark which couples to μ and depend on the branching fractions B_{μ} to the μq final state. The limits are shown for B_{μ} equal to 0.5 and 1

are denoted [8] $S_{1/2}^L, S_{1/2}^R, \tilde{S}_{1/2}^L, V_0^L, V_0^R, \tilde{V}_0^R,$ and $V_{1/2}^L$. For $F = 2$, they are $S_0^L, S_0^R, \tilde{S}_0^R, S_1^L, V_{1/2}^L, V_{1/2}^R,$ and $\tilde{V}_{1/2}^L$. Here S and V indicate scalar and vector leptoquarks respectively, which couple to left- (L) or right-handed (R) leptons as indicated by the superscript. The subscript gives the weak isospin of the LQ³. In s -channel reactions, $F = 0$ LQ cross sections are higher in e^+p collisions, where they are produced via e^+q fusion, than in e^-p collisions where e^-q fusion occurs. The reverse is true for an $F = 2$ leptoquark.

An LQ scenario is defined by the leptoquark species, by the generations of the quarks which couple to the electron and to the final-state lepton, and by the final-state lepton flavor. Hence there are $14 \times 3 \times 3 \times 2 = 252$ different LQ scenarios, each characterized by two dimensionless couplings, λ_{eq_1} and $\lambda_{\ell q_2}$, defined in Fig. 1, which could induce flavor violation. Such LQs would also mediate flavor-conserving interactions with a final-state e or ν_e , which are not considered in this paper.

As an illustration, we show in Fig. 2 the present limits [10] on $\lambda_{eq_1} \lambda_{\ell q_2}$ versus LQ mass, M_{LQ} , for reactions which could proceed through the left-handed scalar isosinglet LQ, S_0^L . Note that each of the limits assumes that specific quark flavors couple to e and μ . For example, the most sensitive limit, from $\mu N \rightarrow e N$, applies only for first-generation quarks in both initial and final states. Also in this figure are the results of direct searches for leptoquark pair production. Searches in e^+e^- collisions at LEP [11] exclude scalar leptoquarks lighter than about 45 GeV which couple to $e, \tau,$ or any neutrino. For leptoquarks with couplings of electromagnetic strength, masses below 73 GeV are excluded. While the LEP experiments did not search for flavor violation, their non-observation of $e\bar{e}q\bar{q}, \mu\bar{\mu}q\bar{q}, \tau\bar{\tau}q\bar{q},$ or $\nu\bar{\nu}q\bar{q}$

³ The tilde differentiates LQ species which differ only in that one species couples to u -type quarks and the other to d -type quarks. See [9] for details

final states kinematically consistent with leptoquark pair production imply flavor-violating leptoquark mass limits which are weaker by at most a few GeV. At the Tevatron [12], searches in $p\bar{p}$ collisions have excluded scalar leptoquarks lighter than 131 GeV (96 GeV) for an assumed branching fraction to $q\mu$ of 100% (50%). These limits on M_{LQ} are independent of the LQ couplings in most models.

The LQ-induced cross sections for reaction (1), given in detail in the appendix, depend on the initial quark density, the couplings, and the species of LQ involved in the reaction, as well as on the kinematic event variables x (the Bjorken scaling variable) and y (the inelasticity). Here x is defined as $x = -q^2/(2q \cdot P)$ and y as $y = (q \cdot P)/(k \cdot P)$, where k, k' , and P are the four-momenta of the initial-state electron, the final-state lepton and the proton respectively, and $q = k - k'$. The square of the center-of-mass energies of the electron-proton and the electron-quark systems are given by $s = (k+P)^2$ and $\hat{s} = xs$ respectively. The remaining Mandelstam variables are given by $t = -sxy$ and $u = -sx(1-y)$.

For a given coupling, the cross section is largest when the LQ mass, M_{LQ} , is less than $\sqrt{\hat{s}}$. In this case, the LQ is produced in the s -channel, as indicated in Fig. 1a. Such a leptoquark will appear as a narrow resonance in the x -distribution peaked at $x_0 \equiv M_{LQ}^2/s$. In the narrow-width approximation described in the appendix, the cross section for this process using unpolarized beams can be written

$$\sigma_{e q_1 \rightarrow \ell q_2} = \frac{\pi}{4s} \lambda_{e q_1}^2 B_{\ell q_2} q_1(x_0, M_{LQ}^2) \int dy f(y), \quad (2)$$

$$\text{where } f(y) = \begin{cases} 1 & \text{scalar LQ} \\ 6(1-y)^2 & \text{vector LQ,} \end{cases}$$

and $q_1(x, M_{LQ}^2)$ is the quark density in the proton for the initial-state quark (or antiquark) flavor q_1 , $\lambda_{e q_1}$ is the coupling at the LQ production vertex and $B_{\ell q_2}$ is the branching fraction of the LQ to lepton ℓ and quark flavor q_2 . In this process, the final state lepton will have a transverse momentum (P_t^ℓ) of order $M_{LQ}/2$.

For resonant s -channel production, the cross section for flavor-violating events is proportional to $\lambda_{e q_1}^2 B_{\ell q_2}$. We will set limits on this quantity as a function of M_{LQ} .

For the case $M_{LQ} \gg \sqrt{\hat{s}}$, either or both s - and u -channel contributions may be important. The corresponding cross sections can be written as

$$\sigma_{e q_1 \rightarrow \ell q_2} = \frac{s}{32\pi} \left[\frac{\lambda_{e q_1} \lambda_{\ell q_2}}{M_{LQ}^2} \right]^2 \int dx dy x q_1(x, \hat{s}) f(y), \quad (3)$$

$$\sigma_{e q_2 \rightarrow \ell q_1} = \frac{s}{32\pi} \left[\frac{\lambda_{e q_1} \lambda_{\ell q_2}}{M_{LQ}^2} \right]^2 \int dx dy x q_2(x, -u) f(y), \quad (4)$$

$$\text{where } f(y) = \begin{cases} \frac{1}{2} & s\text{-channel scalar LQ} \\ \frac{1}{2}(1-y)^2 & u\text{-channel scalar LQ} \\ 2(1-y)^2 & s\text{-channel vector LQ} \\ 2 & u\text{-channel vector LQ,} \end{cases}$$

and the indices q_1 and q_2 specify the quark flavors which couple to the electron and the final-state lepton, respectively. Here the final-state lepton again will have large transverse momentum with $P_t^\ell \approx \sqrt{\hat{s}}/2$.

Notice that in the high-mass case, all information about the leptoquark mass and couplings is contained in the quan-

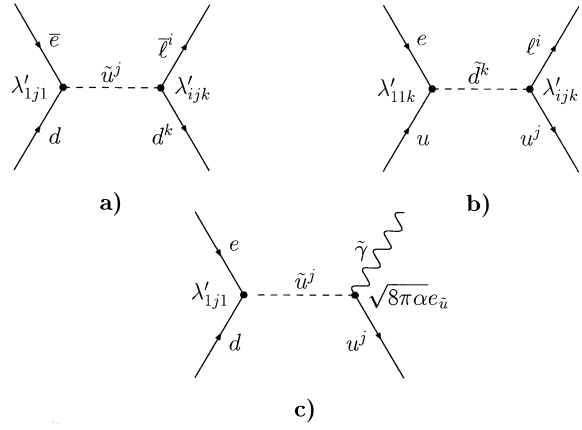


Fig. 3a–c. R_P violating single squark production in ep collisions. Diagrams **a** and **b** show production of \tilde{u} and \tilde{d} squarks with leptoquark-like \tilde{R}_P decays, where ℓ^i denotes the final-state charged lepton of generation i . The indices j and k denote the generations of up-type and down-type (s)quarks respectively. Diagram **c** shows \tilde{u} production with an R_P -conserving decay

tity $\lambda_{e q_1} \lambda_{\ell q_2} / M_{LQ}^2$, which is the quantity on which we set limits. As might be anticipated, other LFV processes mediated by leptoquarks, such as flavor violating meson decays, are sensitive to exactly this quantity. Hence, our results may be compared directly with prior LFV searches. This is done in Sect. 5.

2.2 R -Parity violating squarks

Squarks (\tilde{q}) are the hypothesized supersymmetric partners of quarks. In supersymmetry (SUSY), R -parity is defined as $R_P = (-1)^{3B+L+2S}$ where B, L , and S denote baryon and lepton numbers and spin respectively. This implies that $R_P = +1$ for SM particles and $R_P = -1$ for SUSY particles. If R -parity were conserved, SUSY particles would be produced in pairs and ultimately decay into the lightest supersymmetric particle (LSP), which would be stable and neutral. We refer here to this LSP as the photino ($\tilde{\gamma}$). In a model with R -parity violation, denoted \tilde{R}_P , single SUSY particle production would occur and the LSP would decay into SM particles. Of particular interest for ep collisions are R -parity violating superpotential terms of the form [13] $\lambda'_{ijk} L_L^i Q_L^j \bar{D}_R^k$. Here L_L, Q_L , and \bar{D}_R denote left-handed lepton and quark doublets and the right handed d -quark singlet chiral superfields respectively, and the indices i, j , and k label their respective generations. Expanded into four-component Dirac notation, the corresponding terms of the Lagrangian are

$$\mathcal{L} = \lambda'_{ijk} \left[\bar{\nu}_L^i \bar{d}_R^k d_L^j + \bar{d}_L^j \bar{d}_R^k \nu_L^i + (\bar{d}_R^k)^* (\bar{\nu}_L^i)^c d_L^j - \bar{e}_L^i \bar{d}_R^k u_L^j - \tilde{u}_L^j \bar{d}_R^k e_L^i - (\bar{d}_R^k)^* (\bar{e}_L^i)^c u_L^j \right] + \text{h. c.} \quad (5)$$

For $i = 1$, the last two terms will result in \tilde{u} and \tilde{d} production in ep collisions. Identical terms are found in the Lagrangians for the scalar leptoquarks $\tilde{S}_{1/2}$ and S_0 , respectively [14].

Lepton-flavor violating ep interactions would occur in a model with two non-zero couplings λ'_{ijk} which involve different lepton generations. For example, the process $\bar{e}d \rightarrow$

$\tilde{u}^j \rightarrow \bar{\mu}d^k$ shown in Fig. 3a involves the couplings λ'_{1j1} and λ'_{2jk} . Similarly, non-zero values for λ'_{11k} and λ'_{3jk} would lead to the reaction $e\tilde{u} \rightarrow \tilde{d}^k \rightarrow \tau u^j$ shown in Fig. 3b. Down-type squarks have the additional decay $\tilde{d}^k \rightarrow \nu^i d^j$, a mode unavailable to up-type squarks.

The difference between mechanisms involving R -parity violating squarks and leptoquarks is that the squarks may have additional R -parity conserving decay modes with final-state neutralinos, such as $\tilde{q} \rightarrow q\tilde{\gamma}$ (shown in Fig. 3c) or with final-state charginos, as in $\tilde{u} \rightarrow d\tilde{\chi}^+$. The branching ratios $B_{q\tilde{\gamma}}$ for the R_P -conserving decay $\tilde{q} \rightarrow q\tilde{\gamma}$ and B'_{ijk} for any \mathcal{R}_P decay mode are related [14] by

$$\frac{B'_{ijk}}{(\lambda'_{ijk})^2} = \frac{B_{q\tilde{\gamma}}}{8\pi\alpha e_q^2(1 - m_{\tilde{\gamma}}^2/m_{\tilde{q}}^2)^2}, \quad (6)$$

where λ'_{ijk} is the \mathcal{R}_P coupling at the decay vertex, α is the electromagnetic coupling⁴, e_q is the squark charge in units of the electron charge and the photino and squark masses are $m_{\tilde{\gamma}}$ and $m_{\tilde{q}}$, respectively.

Coupling limits for LFV decays of an S_0^L leptoquark can be interpreted as \tilde{d}^k coupling limits through the correspondence $\lambda_{eq_1}\sqrt{B_{\ell q_2}} = \lambda'_{11k}\sqrt{B'_{ijk}}$ where i and j are the generations of the LQ decay products ℓ and q_2 . Similarly, coupling limits on the $\tilde{S}_{1/2}^L$ LQ can be converted to limits on couplings to \tilde{u}^j via $\lambda_{eq_1}\sqrt{B_{\ell q_2}} = \lambda'_{1j1}\sqrt{B'_{ijk}}$, where i and k are the generations of ℓ and q_2 .

If the stop (\tilde{t}) [15] is lighter than the top quark, then the R_P -conserving decay $\tilde{t} \rightarrow t\tilde{\gamma}$ (Fig. 3c) will not exist. In the case of \tilde{t} , the correspondence with the coupling limit on $\tilde{S}_{1/2}^L$ is given by $\lambda_{ed}\sqrt{B_{\ell q_2}} = \cos\theta_t\lambda'_{131}\sqrt{B'_{i3k}}$ where θ_t is the mixing angle between the SUSY partners of the left- and right-handed top quarks. Over a broad range of possible stop masses, it is expected that $\cos^2\theta_t \sim 0.5$ [15].

3 The ZEUS detector and event simulation

The main components of the ZEUS detector [16] used for this analysis were the uranium-scintillator calorimeter (CAL) [17] and the central tracking detector (CTD) [18].

The CAL, which covers polar angles⁵ between 2.2° and 176.5° , is divided into forward (FCAL), barrel (BCAL), and rear (RCAL) parts. Each part is further subdivided into towers which are longitudinally segmented into electromagnetic (EMC) and hadronic (HAC) sections. In depth, the EMC is one interaction length; the HAC sections vary from six to three interaction lengths, depending on polar angle. Under test beam conditions [17], the calorimeter has an energy resolution of $\sigma_E(\text{GeV}) = 0.18\sqrt{E(\text{GeV})}$ for electrons and $\sigma_E(\text{GeV}) = 0.35\sqrt{E(\text{GeV})}$ for hadrons. In this analysis, only cells with energies above noise suppression thresholds (60 MeV for EMC, 110 MeV for HAC) were used.

⁴ We evaluate α at the scale M_Z ($\alpha=1/128$) because \hat{s} is of order M_Z at HERA

⁵ The ZEUS coordinate system is right-handed with the Z axis pointing in the proton beam direction, hereafter referred to as forward, and the X axis horizontal, pointing toward the center of HERA. The polar angle θ is taken with respect to the proton beam direction from the interaction point

A superconducting coil located inside the CAL provides a 1.43 Tesla magnetic field parallel to the beam axis in which the charged particle tracking system operated. The interaction vertex is reconstructed with a resolution of 4 mm (1 mm) along (transverse to) the beam direction. The muon detection system [19] was used to check the efficiencies and the background estimates for the primary muon identification, which used only the CAL and the CTD. The muon detectors are also divided into three sections covering the forward, barrel, and rear regions. In the barrel and rear sections, which were used for this analysis, the detectors consist of eight layers of limited streamer tubes, four layers on each side of the 80 cm thick magnetized iron yoke. Luminosity was measured [20] from the rate of bremsstrahlung events ($ep \rightarrow ep\gamma$) detected by a photon calorimeter (LUMI) located downstream of the main detector. The luminosity is known to 3% for the e^-p data and to 2% for the e^+p data.

To evaluate detection efficiencies, we have simulated flavor-violating LQ processes using a modified⁶ version of PYTHIA [21] and also with LQMGEN which is based on the differential LQ cross-sections given in [9]. The calculations included initial state bremsstrahlung.

For background estimation, charged-current (CC) and neutral-current (NC) deep-inelastic scattering (DIS) events with electroweak radiative corrections were simulated using LEPTO [22] interfaced to HERACLES [23] via DJANGO [24]. The MRSA [25] parton density parameterization was used. The hadronic final state was simulated using ARIADNE [26] and JETSET [21].

Photoproduction processes were simulated using HERWIG [27], and photoproduction of $c\bar{c}$ and $b\bar{b}$ pairs by PYTHIA and AROMA [28]. The processes $\gamma\gamma \rightarrow \mu^+\mu^-$ and $\gamma\gamma \rightarrow \tau^+\tau^-$ were generated using ZLPAIR [29]. Finally, production of W bosons was simulated using EPEVC [30].

All generated events were passed through a GEANT [31] based detector simulation which tracked final state particles and their decay and interaction products through the entire detector. The simulated events were processed with the same analysis programs as the data.

4 Trigger and analysis

The signature of LFV events ($e+p \rightarrow \ell+X$) in this experiment is an isolated μ or τ of high transverse momentum, $P_t^\ell \sim \sqrt{\hat{s}}/2$, balanced by a jet of hadrons.

4.1 Search strategy

Our search strategy relies on the fact that the LFV signal events will almost always have a large net transverse momentum \cancel{P}_t^{cal} measured in the calorimeter. We reconstruct \cancel{P}_t^{cal} as $\cancel{P}_t^{cal} = (P_X^2 + P_Y^2)^{1/2}$. Here $P_X = \sum_i E_i \sin(\theta_i) \times \cos(\phi_i)$ and $P_Y = \sum_i E_i \sin(\theta_i) \sin(\phi_i)$ where the sums run over all calorimeter cells and E_i , θ_i , and ϕ_i are the energy, polar angle and azimuthal angle of cell i , calculated

⁶ The final-state electron and quark from these generators were replaced by the appropriate lepton (μ or τ), and quark species, before the simulation of parton showering and fragmentation. Both s - and u -channel exchange contributions were included

using the reconstructed event vertex. We also reconstruct the azimuth of the missing transverse momentum, determined from $\cos \phi_{miss} = -P_X / \cancel{p}_t^{cal}$ and $\sin \phi_{miss} = -P_Y / \cancel{p}_t^{cal}$.

A high energy muon is a minimum ionizing particle, typically producing a measured energy of about 2 GeV in the calorimeter. If the much larger muon transverse momentum, P_t^μ , is balanced by a jet of hadrons, then $\cancel{p}_t^{cal} \approx P_t^\mu$. Thus the signature for such an event would be a large \cancel{p}_t^{cal} and a high momentum track which points to an isolated calorimeter cluster with approximately 2 GeV of energy at an azimuthal angle ϕ_{miss} .

A final-state τ decays promptly to a small number of charged particles (1 or 3, 99.9% of the time), zero or more neutral hadrons, and at least one neutrino. Since the τ mass is small ($m_\tau = 1.78$ GeV) compared to its transverse momentum, the τ decay products will be collimated in a cone of opening angle ~ 0.03 radians. For events in which the τ decays via $\tau \rightarrow \mu\nu\bar{\nu}$, the experimental signature will be similar to an event with a final state muon except with $P_t^\mu < \cancel{p}_t^{cal}$. If the τ decays via $\tau \rightarrow e\nu\bar{\nu}$, the event will be characterized by large \cancel{p}_t^{cal} (due to the undetected neutrinos) and the presence of a high-transverse-momentum electron with azimuth ϕ_{miss} . Finally, in the case of a hadronic τ decay, we would again see a large \cancel{p}_t^{cal} due to the neutrino, and a compact hadronic cluster with 1 or 3 tracks, also at azimuth ϕ_{miss} .

4.2 Trigger

Data were collected with a three-level trigger system [16]. Since the signature which we are seeking is one with missing transverse momentum measured in the calorimeter, our triggering scheme was largely calorimeter based. The first-level triggers used net transverse energy, missing transverse energy, as well as EMC energy sums in the calorimeter. The thresholds were well below the offline requirements. The second-level trigger rejected backgrounds (mostly p -gas interactions and cosmic rays) for which the calorimeter timing was inconsistent with an ep interaction. Events were accepted if \cancel{p}_t^{cal} exceeded 9 GeV and either a track was found in the CTD or at least 10 GeV was deposited in the FCAL. The latter alternative was intended to accept events with jets which are too forward for the tracks to be observed in the CTD. The third-level trigger applied stricter timing cuts and also pattern recognition algorithms to reject cosmic rays.

4.3 Leptoquark mass reconstruction

For $M_{LQ} < 300$ GeV, the leptoquark is produced as an s -channel resonance and consequently, the invariant mass distribution of the $q\ell$ final state is sharply peaked at M_{LQ} . When searching for a leptoquark of a given mass, the expected background can be reduced by requiring the reconstructed $q\ell$ mass to be consistent with M_{LQ} .

We reconstruct the leptoquark mass as follows using a simple ansatz based on three approximations: 1) the four-momentum of all final state muons and neutrinos can be represented by a single massless pseudoparticle; 2) the contribution of the proton remnant to the reconstructed mass

can be ignored; and 3) no energy escapes through the rear beam hole.

The four-momentum of the invisible pseudoparticle, P^{invis} , is related to the net four-momentum $P = (E, P_X, P_Y, P_Z)$ measured in the calorimeter as $P_X^{invis} = -P_X$, $P_Y^{invis} = -P_Y$, and $E - P_Z + E^{invis} - P_Z^{invis} = 2E_e$ where E_e is the electron beam energy. The reconstructed leptoquark mass is given by $(M_{LQ}^{rec})^2 = (P + P^{invis})^2$.

We have applied this mass reconstruction to simulated LFV events and determined two functions, $\mu_{LQ}^{rec}(M_{LQ})$ and $\sigma_{LQ}^{rec}(M_{LQ})$ which give the mean and the standard deviation of a Gaussian fit to the reconstructed mass distribution as a function of the true M_{LQ} . Studies of simulated LQ signals indicate that the mass resolution improves from about 13% at $M_{LQ} = 100$ GeV, to about 6% at $M_{LQ} = 250$ GeV.

4.4 Event selection

The most important offline selection requires that \cancel{p}_t^{cal} exceed 12 GeV. The initial event selection is designed to accept all ep collisions which meet this condition, while efficiently rejecting the high-rate backgrounds from cosmic rays, proton-gas interactions, off-beam protons, and beam-halo muons. Triggers from these backgrounds usually do not have a reconstructed vertex. In cases where a spurious vertex is reconstructed, it typically is made from a small number of low-momentum spiraling tracks which do not intersect with the beam line. Unlike ep collisions, for which the distribution of Z vertex position is centered at $Z = 0$ with an r. m. s. width of 12 cm, the spurious vertices have a Z distribution which is roughly uniform. In cases of protons colliding with residual gas in the beam pipe, or with the beam-pipe itself, the low-multiplicity spurious vertex is accompanied by a large number (10 to 100) of tracks which are not correlated with the vertex. Occasionally a cosmic ray or a beam-halo muon will coincide with an ep interaction which provides the reconstructed vertex. In these cases the vertex tracks are typically of quite low momentum ($\mathcal{O}(100$ MeV)).

In order to remove such backgrounds, we require that a vertex is reconstructed and that it lie within 50 cm of the nominal interaction point. We define N_{trk} to be the total number of reconstructed tracks, N_{good} to be the number of tracks with transverse momentum $P_t > 300$ MeV and a distance of closest approach to the beam-line of less than 1.5 cm, and N_{vtx} to be the number of tracks forming the vertex. We require $N_{good} \geq 1$ and $N_{good} \geq 0.05N_{trk}$. In order to reject proton-induced background, for which the energy deposited in the calorimeter is concentrated at small polar angles, we remove events with $P_Z/E > 0.8(0.94)^7$ if $N_{trk} - N_{vtx} \geq 80$ (20). In addition, we require the timing of each calorimeter cluster with energy above 2 GeV to be consistent with an ep interaction. To reduce the cosmic ray background, we apply an algorithm which rejects events in which the pattern of calorimeter energy deposits is consistent with a single penetrating particle traversing the detector.

The 175 events which passed these cuts were visually examined and 29 events clearly initiated by cosmic rays,

⁷ Here P_Z and E are reconstructed from the calorimeter cells in a manner similar to the components P_X and P_Y described above

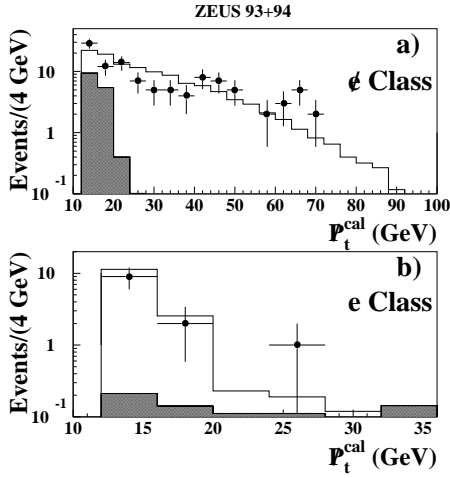


Fig. 4a,b. Net transverse momentum (p_t^{cal}) distribution of events in the class ϕ sample (a) and the class e sample (b). The points represent the data. The solid lines show the Monte Carlo prediction, which includes CC DIS, NC DIS, resolved and direct photoproduction and $\gamma\gamma$ interactions. In the top plot, the shaded region shows the Monte Carlo prediction for all processes except CC DIS. In the bottom plot, the shaded region shows the Monte Carlo prediction for all processes except NC DIS

muons in the beam halo, or anomalous photomultiplier discharges were removed, leaving 146 ep collision events. These events were divided into two classes: those for which no isolated electron with energy $E_e > 10$ GeV was found in the calorimeter (class ϕ); and those for which such an electron was found (class e). The following selection cuts, which were developed in Monte Carlo studies, were applied to each sample in order to eliminate SM backgrounds.

ϕ : There were 114 events with no isolated electron. Six events were rejected because an electron of more than 5 GeV was observed in the luminosity electron calorimeter and they were thus recognized to be background due to photon-proton (γp) collisions. This left 108 ϕ events, which agrees well with the Monte Carlo estimates of 100 CC DIS events and 15 γp and $\gamma\gamma$ events. The p_t^{cal} distribution of this ϕ sample is compared with the Monte Carlo prediction in Fig. 4a. The ϕ sample serves as the source of flavor violation candidates with a muon in the final state, as well as of candidates with final-state τ 's which subsequently decay via $\tau \rightarrow \mu\bar{\nu}\nu$ or $\tau \rightarrow \nu$ +hadrons.

e : There were 32 events which contained an isolated electron. In order to reject NC DIS background, for which the electrons are concentrated at large polar angles, we required the electron polar angle to be less than 100° . After this cut, 12 events remained in the e sample, compatible with the Monte Carlo prediction of 14 NC DIS events. The p_t^{cal} distribution of these remaining events is compared with the Monte Carlo prediction in Fig. 4b. LFV candidates with a final-state τ which decays via $\tau \rightarrow e\bar{\nu}\nu$ (18% branching fraction) were sought in this sample.

The final cuts rely on a clustering algorithm⁸ which assigns each calorimeter cell above noise threshold to one and

⁸ The clustering algorithm joins each cell with its highest energy neighbor, thus producing one cluster for each cell which has more energy than any of its neighbors. Two cells are defined as neighbors if they are in towers

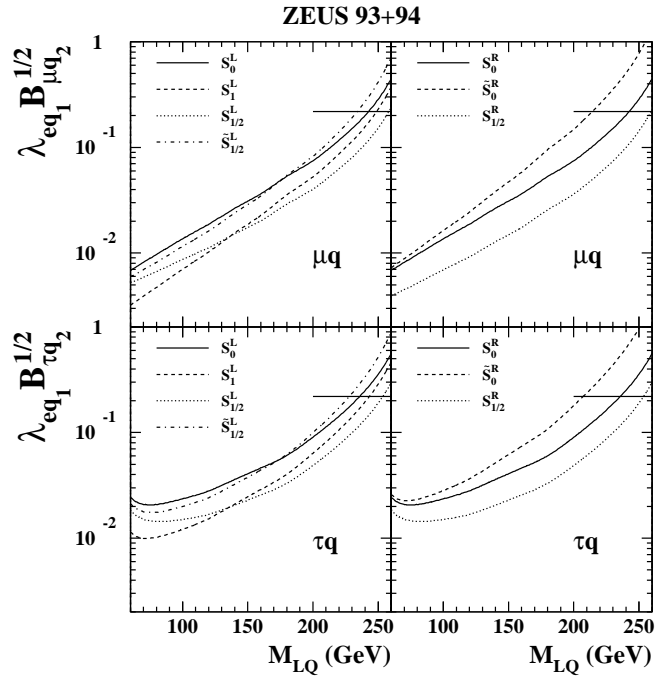


Fig. 5. The upper limit on the coupling at the production vertex (λ_{eq_1}) times the square root of the branching fraction to the μq or τq final state ($B_{\ell q_2}$) vs. leptoquark mass M_{LQ} , at 95% CL for scalar leptoquarks. The horizontal line indicates nominal electromagnetic coupling ($\lambda_{eq_1}^2 = 4\pi\alpha = 4\pi/128$) and $B_{\ell q_2} = 0.5$

only one cluster. Each cluster is characterized by its energy, E_{clu} , as well as the energy-weighted mean azimuth, ϕ_{clu} , and pseudorapidity, $\eta_{clu} = -\ln[\tan(\theta_{clu}/2)]$. We expect the final-state lepton in a LFV event to produce a single isolated cluster. To decide if a cluster is isolated, we examine the set of all calorimeter cells which are within 0.8 units in $\eta\phi$ of the cluster ($[(\phi_{clu} - \phi_{cell})^2 + (\eta_{clu} - \eta_{cell})^2]^{1/2} < 0.8$). A cluster is defined to be *isolated* if the summed energy of all calorimeter cells in this set which do not belong to the cluster is below 2 GeV. For each cluster, we also compute $\overline{\phi_{clu}}$, which is defined as the energy weighted mean azimuth of all cells in the entire calorimeter, except for those assigned to the cluster. Note that for LFV events $\overline{\phi_{clu}}$ differs only slightly from $\overline{\phi_{miss}}$ which is computed using all calorimeter cells. A cluster is said to be p_t^{cal} -aligned if it satisfies the inequality: $\cos(\phi_{clu} - \overline{\phi_{clu}}) < \cos 170^\circ$. This ensures that the isolated cluster is opposite in azimuth to the rest of the energy in the calorimeter.

To enter the final sample for μq or τq final states, an event must satisfy the criteria of one of four selections, described below.

μ or $\tau \rightarrow \mu$: In a class ϕ event, there must exist an isolated p_t^{cal} -aligned cluster with energy $0.5 \text{ GeV} < E_{clu} < 6 \text{ GeV}$ and at most 80% of its energy in the electromagnetic layer of the calorimeter. It must have exactly one

which share a face or an edge. Cells on the forward or rear edges of the BCAL are also neighbors with the FCAL or RCAL cells which are behind them, as viewed from the interaction point

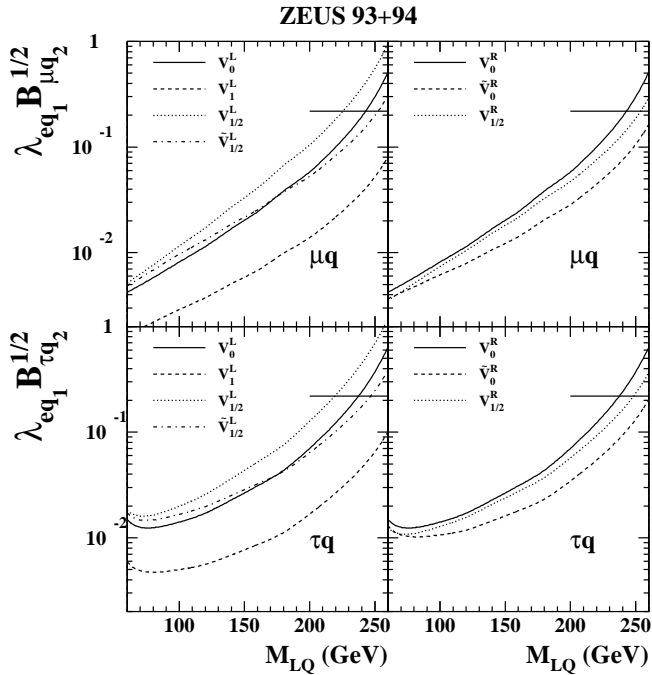


Fig. 6. The upper limit on the coupling at the production vertex (λ_{eq_1}) times the square root of the branching fraction to the μq or τq final state ($B_{\ell q_2}$) vs. leptoquark mass M_{LQ} , at 95% CL for vector leptoquarks. The horizontal line indicates nominal electromagnetic coupling ($\lambda_{eq_1}^2 = 4\pi\alpha = 4\pi/128$) and $B_{\ell q_2} = 0.5$.

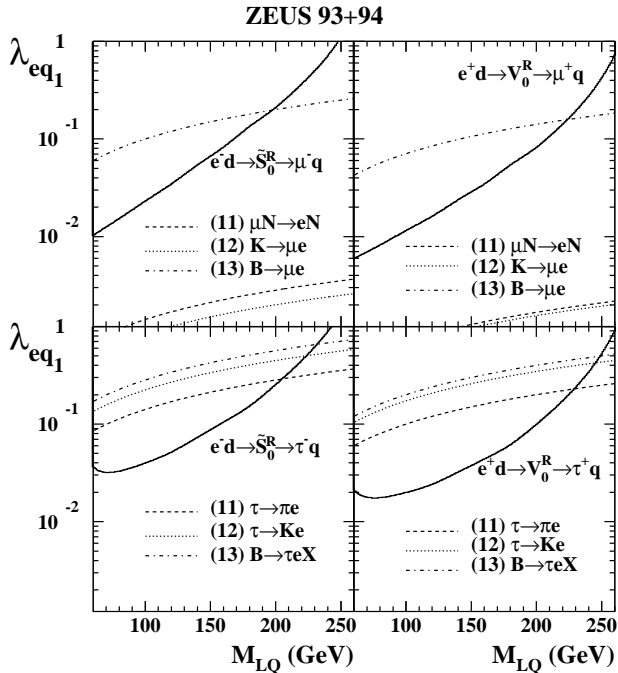


Fig. 7. The 95% CL upper limits on λ_{eq_1} vs. leptoquark mass M_{LQ} , for selected LQ species which decay to ℓq , where $\ell = \mu$ (above) or τ (below), assuming $B_{\ell q_2} = 0.5$. The solid curves are ZEUS results and the various broken curves show existing limits [10]. Paired numbers in parentheses indicate the generations of the quarks which couple to e and ℓ respectively.

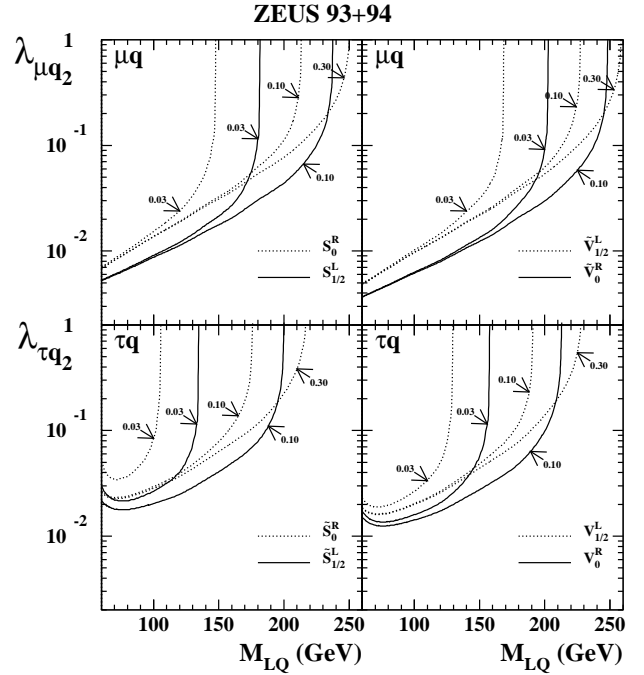


Fig. 8. The upper limit on the coupling at the decay vertex ($\lambda_{\ell q_2}$) vs. leptoquark mass M_{LQ} , for several values of the first-generation coupling at the production vertex (λ_{eq_1}). Each curve is labeled by the value of λ_{eq_1} . The dotted curves are for $F = 2$ leptoquarks and the solid curves are for $F = 0$ leptoquarks.

Table 1. The 95% confidence level lower limits on the LQ mass (GeV) for nominal electromagnetic coupling. For leptoquarks which couple to μ , we set $\lambda_{eq_1}^2 = \lambda_{\mu q_2}^2 = 4\pi\alpha$. For leptoquarks which couple to τ , we set $\lambda_{eq_1}^2 = \lambda_{\tau q_2}^2 = 4\pi\alpha$. Limits are shown for all scalar (S) and vector (V) leptoquark species

LQ species	S_0^L	S_0^R	\tilde{S}_0^R	$S_{1/2}^L$	$S_{1/2}^R$	$\tilde{S}_{1/2}^L$	S_1^L
μq	231	242	214	258	259	234	243
τq	223	236	207	253	254	228	236

LQ species	V_0^L	V_0^R	\tilde{V}_0^R	$V_{1/2}^L$	$V_{1/2}^R$	$\tilde{V}_{1/2}^L$	V_1^L
μq	234	243	264	225	254	252	272
τq	227	237	261	219	248	246	270

matching track⁹ and that track must have momentum exceeding 20 GeV. The efficiency¹⁰ to satisfy these cuts for scalar (vector) leptoquarks which decay to μq decreases with LQ mass from 74% (78%) at $M_{LQ} = 80$ GeV to 31% (50%) at $M_{LQ} = 260$ GeV. The background estimate for the μ selection was 0.1 events from the inelastic process $\gamma\gamma \rightarrow \mu^+\mu^-$. Zero events were observed in the data.

To check the efficiency of the muon selection, we performed an independent event selection which did not use the CAL, but required a track in the barrel or rear muon chambers which was matched to a CTD track with a transverse momentum of at least 5 GeV. In order to select events with isolated muons, we rejected events

⁹ A matching track is defined such that the distance of closest approach between the extrapolated track and the calorimeter cluster is less than 30 cm

¹⁰ All quoted efficiencies include the trigger efficiency

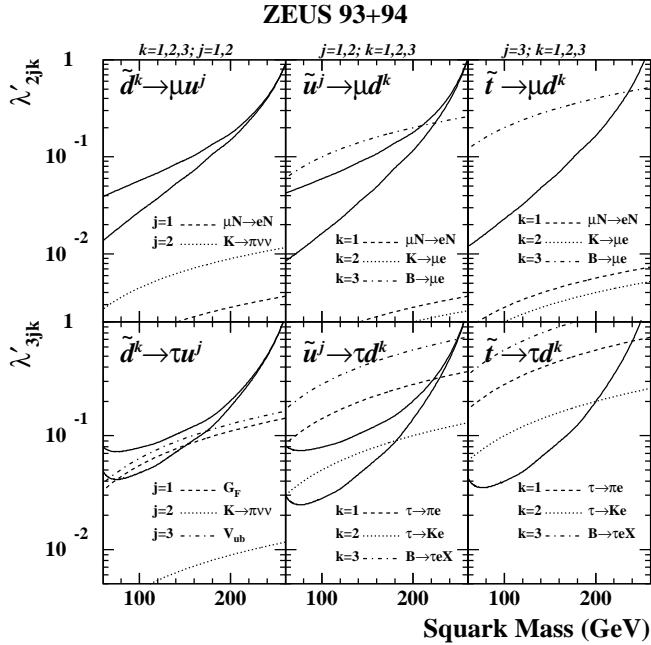


Fig. 9. Limits on the \mathcal{R}_P coupling λ'_{ijk} at 95% CL for squarks which decay to μq ($i = 2$) or τq ($i = 3$). For \tilde{d} limits, we assume that $\lambda'_{11k} = \lambda'_{ijk}$, while for \tilde{u} (including \tilde{t}) limits, we assume that $\lambda'_{1j1} = \lambda'_{ijk}$. The *lower solid curves* give the ZEUS limits for squarks which decay purely via R -parity violation. The *upper solid curves* give the ZEUS limits for the case where, in addition, the gauge decay $\tilde{q} \rightarrow q\tilde{\gamma}$ exists, and where the photino is much lighter than the squark. In the case of \tilde{t} , we only consider \mathcal{R}_P decays and assume that the stop mixing angle is given by $\cos^2 \theta_t = 0.5$. The values of j and k for which each limit applies are indicated above the plots. The *dashed and dotted curves* show the limits from other experiments (adapted from [10]). These limits depend on the generation of the quark which couples to the μ or τ as indicated

which had an electron found in the calorimeter or had more than three tracks fitted to the vertex. A total of 15 events, which contained 17 CTD-matched muon chamber tracks passed these cuts. This number agrees with the Monte Carlo estimate of 20 events from $\gamma\gamma \rightarrow \mu^+\mu^-$. All 17 tracks were matched to an isolated calorimeter cluster which passed the cuts described above (except for the \not{p}_t^{cal} -alignment).

$\tau \rightarrow e$: In a class e event, the isolated electron must be \not{p}_t^{cal} -aligned. The efficiency to satisfy these cuts for scalar (vector) leptoquarks with final-state τq , and the subsequent decay $\tau \rightarrow e\nu\nu$, rises with LQ mass from 23% (17%) at $M_{LQ} = 80$ GeV to 75% (75%) at $M_{LQ} = 260$ GeV. The background estimate for the $\tau \rightarrow e$ selection was 0.2 events from NC DIS. Zero events were observed in the data.

$\tau \rightarrow$ hadrons: In a class \not{e} event, there must exist an isolated \not{p}_t^{cal} -aligned cluster with $E_{clu} > 10$ GeV, which has either 1 or 3 matching tracks. At least one track must have a momentum exceeding 5 GeV. The efficiency to satisfy these cuts for scalar (vector) leptoquarks with final-state τq and hadronic τ decay rises with leptoquark mass from 15% (12%) at $M_{LQ} = 80$ GeV to 39% (47%) at $M_{LQ} = 260$ GeV. We estimated a background of 0.4 events for this selection coming from CC DIS (0.2

event), $\gamma\gamma \rightarrow \mu^+\mu^-$ (0.1 event), and $c\bar{c}$ production (0.1 event). We observed zero events.

$\not{p}_t^{cal} > 80$ GeV: Leptoquarks with mass in the range $200 \text{ GeV} < M_{LQ} < 300$ GeV would be strongly boosted in the forward direction so that the final state μ or τ would often have polar angle less than 10° . In such cases, the final-state lepton would be outside the CTD acceptance and would consequently fail the track matching cuts. In order to maintain high efficiency at these masses, we accept *any* event from either class e or class \not{e} for which $\not{p}_t^{cal} > 80$ GeV. For 240 GeV leptoquarks which decay to μq , accepting events with $\not{p}_t^{cal} > 80$ GeV increases the overall acceptance from 36% to 69% for scalars, and from 53% to 76% for vectors. For the $\not{p}_t^{cal} > 80$ GeV selection, we estimated a background of 1.0 events from CC DIS and we observed zero events.

For the low-mass leptoquark search ($M_{LQ} < 300$ GeV), one additional cut was applied, which, in contrast to all cuts described above, depends on M_{LQ} , the mass of the LQ being searched for. The leptoquark mass was reconstructed using the method described in 4.3 and we required that the reconstructed mass must lie within $3\sigma_{LQ}^{rec}(M_{LQ})$ of $\mu_{LQ}^{rec}(M_{LQ})$.

5 Results

With no candidate events for LFV found in either the e^-p or e^+p data samples with integrated luminosities $\mathcal{L}_{e^-} = 0.84 \text{ pb}^{-1}$ and $\mathcal{L}_{e^+} = 2.94 \text{ pb}^{-1}$, we set upper limits on the couplings of the various LFV processes described in Sect. 2. The upper limit on the coupling λ is obtained from the relation $N = \sum_{i=e^+,e^-} \mathcal{L}_i \epsilon_i \sigma_i(\lambda)$, where ϵ is the efficiency, $\sigma(\lambda)$ is the cross section for a coupling λ , and N is the Poisson 95% confidence level (CL) upper limit [32] on the number of events. The signal efficiencies and background estimates were determined by Monte Carlo studies. We estimate the systematic uncertainties in the efficiencies to be 5%. Cross sections were calculated using the formulae given in the appendix and the GRV-HO [33] parton density parameterization. Cross sections calculated using the MRSB [34] parameterization differ in magnitude by less than 12% for u, d, s , or c quarks in the initial state, and by less than 19% for initial-state b quarks.

5.1 Low-mass leptoquark limits ($M_{LQ} < 300$ GeV)

In the case of low-mass leptoquarks, we calculate upper limits on $\lambda_{eq_1}^2 B_{\ell q_2}$ using equation 2. Since our limits are largely independent of the final state quark type (as long as the top quark is not involved), we show in Figs. 5 and 6 the upper limits on $\lambda_{eq_1} \sqrt{B_{\ell q_2}}$, for scalar and vector leptoquarks where q_1 is a first-generation quark and q_2 is the final-state quark of any generation (except top). The limits for $\ell = \mu$ and for $\ell = \tau$ are shown separately as a function of LQ mass for the various scalar and vector LQ species. We note that for several LQ species, we probe coupling strengths as small as $\lambda_{eq_1}^2/4\pi \approx 10^{-3}\alpha$ for $M_{LQ} = 100$ GeV and $B_{\ell q_2} = 0.5$.

In Fig. 7 we compare these limits on LFV with those from previous searches for two representative LQ species,

Table 2. The best upper bounds on $\lambda_{eq_1}\lambda_{\mu q_2}/M_{LQ}^2$ for $F = 2$ leptoquarks, in units of 10^{-4} GeV^{-2} . Each column corresponds to a given leptoquark species and each row to the quark flavors q_1 and q_2 which couple to e and μ , the generation indices of which are specified in the first column. The top line in each box gives the previous measurement [10] which had obtained the strictest limit. The limit from that experiment is given on the second line in the box and the ZEUS limit, shown on the third line, is printed in boldface if it supersedes the previous limit. The asterisks denote those cases where lepton flavor violation occurs only via processes involving top

		$e \leftrightarrow \mu$			$F = 2$		
$(q_1 q_2)$	S_0^L	S_0^R	\tilde{S}_0^R	S_1^L	$V_{1/2}^L$	$V_{1/2}^R$	$\tilde{V}_{1/2}^L$
	$e^- u$	$e^- u$	$e^- d$	$e^-(u + \sqrt{2}d)$	$e^- d$	$e^-(u + d)$	$e^- u$
	νd			$\nu(\sqrt{2}u + d)$	νd		νu
(11)	$\mu N \rightarrow eN$ 2×10^{-6} 0.09	$\mu N \rightarrow eN$ 2×10^{-6} 0.09	$\mu N \rightarrow eN$ 2×10^{-6} 0.12	$\mu N \rightarrow eN$ 5×10^{-7} 0.05	$\mu N \rightarrow eN$ 7×10^{-7} 0.05	$\mu N \rightarrow eN$ 4×10^{-7} 0.03	$\mu N \rightarrow eN$ 7×10^{-7} 0.04
(12)	$K \rightarrow \pi \bar{\nu} \nu$ 2×10^{-5} 0.12	$D \rightarrow \mu \bar{e}$ 0.14 0.12	$K \rightarrow \mu \bar{e}$ 10^{-6} 0.14	$K \rightarrow \mu \bar{e}$ 6×10^{-7} 0.06	$K \rightarrow \mu \bar{e}$ 6×10^{-7} 0.09	$K \rightarrow \mu \bar{e}$ 6×10^{-7} 0.06	$D \rightarrow \mu \bar{e}$ 0.07 0.08
(13)	V_{ub} 0.004	*	$B \rightarrow \mu \bar{e}$ 0.01 0.15	V_{ub} 0.004 0.07	$B \rightarrow \mu \bar{e}$ 0.005 0.10	$B \rightarrow \mu \bar{e}$ 0.005 0.10	*
(21)	$K \rightarrow \pi \bar{\nu} \nu$ 2×10^{-5} 0.12	$D \rightarrow \mu \bar{e}$ 0.14 0.12	$K \rightarrow \mu \bar{e}$ 10^{-6} 0.14	$K \rightarrow \mu \bar{e}$ 6×10^{-7} 0.06	$K \rightarrow \mu \bar{e}$ 6×10^{-7} 0.05	$K \rightarrow \mu \bar{e}$ 6×10^{-7} 0.03	$D \rightarrow \mu \bar{e}$ 0.07 0.04
(22)	$\mu \rightarrow e\gamma$ 2×10^{-4} 0.24	$\mu \rightarrow e\gamma$ 2×10^{-4} 0.24	$\mu \rightarrow e\gamma$ 8×10^{-5} 0.20	$\mu \rightarrow e\gamma$ 4×10^{-5} 0.09	$\mu \rightarrow e\gamma$ 0.10	$\mu \rightarrow e\gamma$ 6×10^{-3} 0.08	$\mu \rightarrow e\gamma$ 6×10^{-3} 0.13
(23)	$B \rightarrow \ell \nu X$ 0.04	*	$B \rightarrow \bar{\mu} e K$ 6×10^{-3} 0.21	$B \rightarrow \bar{\mu} e K$ 3×10^{-3} 0.11	$B \rightarrow \bar{\mu} e K$ 3×10^{-3} 0.13	$B \rightarrow \bar{\mu} e K$ 3×10^{-3} 0.13	*
(31)	V_{ub} 0.004	*	$B \rightarrow \mu \bar{e}$ 0.01 0.16	V_{ub} 0.004 0.08	$B \rightarrow \mu \bar{e}$ 0.005 0.05	$B \rightarrow \mu \bar{e}$ 0.005 0.05	*
(32)	$B \rightarrow \ell \nu X$ 0.04	*	$B \rightarrow \bar{\mu} e K$ 6×10^{-3} 0.26	$B \rightarrow \bar{\mu} e K$ 3×10^{-3} 0.13	$B \rightarrow \bar{\mu} e K$ 3×10^{-3} 0.11	$B \rightarrow \bar{\mu} e K$ 3×10^{-3} 0.11	*
(33)		*	$\mu \rightarrow e\gamma$ 8×10^{-5} 0.29	$\mu \rightarrow e\gamma$ 4×10^{-5} 0.14	$\mu \rightarrow e\gamma$ 0.01 0.15	$\mu \rightarrow e\gamma$ 0.01 0.15	*

\tilde{S}_0^R and V_0^R . Assuming that $B_{\ell q_2} = 0.5$, we plot as a solid curve the upper limit on λ_{eq_1} as a function of the LQ mass. Curves are shown for both μ (upper plots) and τ (lower plots) final states. In contrast with many other limits on LFV, the coupling limits from this experiment apply to final-state quarks of any generation (except top). The various broken curves are low-energy limits quoted from reference [10]. For each of these curves, the pairs of numbers in parentheses denote the generations of quarks which couple to e and ℓ . Coupling limits for $B_{\ell q} \neq 0.5$ can be obtained by multiplying the limit on λ_{eq_1} plotted in Fig. 7 by $\sqrt{0.5/B_{\ell q}}$. We emphasize two important implications of Fig. 7:

1. The ZEUS limits on $ed \rightarrow \mu b$ via \tilde{S}_0^R (V_0^R) for $M_{LQ} < \sqrt{s}$ supersede previous upper bounds [37] from $B \rightarrow \mu \bar{e}$, for M_{LQ} below 200 GeV (220 GeV). On the other hand, the limits from μ conversion in titanium [1] and from forbidden K decays [3] which involve only first and second generation quarks are much stronger than the corresponding ZEUS limits.
2. For M_{LQ} below 200 GeV, the ZEUS limits on $ed \rightarrow \tau q_2$ through \tilde{S}_0^R and V_0^R supersede previous limits from $\tau \rightarrow \pi e$ [35], $\tau \rightarrow Ke$ [36], and $B \rightarrow \tau e X$ [37], for $q_2 = d, s$, and b , respectively.

Figure 7 illustrates examples in which the existing low-energy limits, though less stringent than the ZEUS limits at low M_{LQ} , become more stringent at higher masses. As described in the next section, this is not always the case.

An alternative approach to setting limits, which was employed in reference [7] is to assume that the branching ratio $B_{\ell q_2}$ is given¹¹ by $\lambda_{\ell q_2}^2 / (\lambda_{eq_1}^2 + \lambda_{\ell q_2}^2)$, and to set limits on $\lambda_{\ell q_2}$ for a fixed value of λ_{eq_1} . Such limits are shown in Fig. 8. For $F = 0$ LQs, our limits are similar to those of reference [7], while for $F = 2$ LQs, the ZEUS limits are stronger due to inclusion of $e^- p$ data.

Finally, a third way to illustrate the sensitivity is to assume that the LQ couplings have electromagnetic strength ($\lambda_{eq_1}^2 = \lambda_{\mu q_2}^2 = 4\pi\alpha$ for LQs which couple to e and μ) and to determine a lower limit on the allowed LQ mass. Such limits are shown in Table 1. For scalar leptoquarks, lower mass limits between 207 GeV and 259 GeV are set. Somewhat stronger mass limits, between 219 GeV and 272 GeV, are set on vector leptoquarks for which both the production cross section and detection efficiency are higher.

¹¹ This formula for $B_{\ell q_2}$ assumes that the leptoquark does not couple to neutrinos

Table 3. The best upper bounds on $\lambda_{eq_1}\lambda_{\mu q_2}/M_{LQ}^2$ for $F = 0$ leptoquarks, in units of 10^{-4} GeV^{-2} . Each column corresponds to a given leptoquark species and each row to the quark flavors q_1 and q_2 which couple to e and μ , the generation indices of which are specified in the first column. The top line in each box gives the previous measurement [10] which had obtained the strictest limit. The limit from that experiment is given on the second line in the box and the ZEUS limit, shown on the third line, is printed in boldface if it supersedes the previous limit. The asterisks denote those cases where lepton flavor violation occurs only via processes involving top

		$e \leftrightarrow \mu$				$F = 0$	
$(q_1 q_2)$	$S_{1/2}^L$ $e^- \bar{u}$ $\nu \bar{u}$	$S_{1/2}^R$ $e^- (\bar{u} + \bar{d})$	$\tilde{S}_{1/2}^L$ $e^- \bar{d}$ $\nu \bar{d}$	V_0^L $e^- \bar{d}$ $\nu \bar{u}$	V_0^R $e^- \bar{d}$	\tilde{V}_0^R $e^- \bar{u}$	V_1^L $e^- (\sqrt{2}\bar{u} + \bar{d})$ $\nu (\bar{u} + \sqrt{2}\bar{d})$
(11)	$\mu N \rightarrow e N$ 2×10^{-6} 0.07	$\mu N \rightarrow e N$ 7×10^{-7} 0.06	$\mu N \rightarrow e N$ 2×10^{-6} 0.10	$\mu N \rightarrow e N$ 7×10^{-7} 0.06	$\mu N \rightarrow e N$ 7×10^{-7} 0.06	$\mu N \rightarrow e N$ 7×10^{-7} 0.04	$\mu N \rightarrow e N$ 3×10^{-7} 0.02
(12)	$D \rightarrow \mu \bar{e}$ 0.14 0.08	$K \rightarrow \mu \bar{e}$ 10^{-6} 0.06	$K \rightarrow \mu \bar{e}$ 10^{-6} 0.10	$K \rightarrow \mu \bar{e}$ 6×10^{-7} 0.07	$K \rightarrow \mu \bar{e}$ 6×10^{-7} 0.07	$D \rightarrow \mu \bar{e}$ 0.07 0.06	$K \rightarrow \mu \bar{e}$ 6×10^{-7} 0.03
(13)	*	$B \rightarrow \mu \bar{e}$ 0.01 0.11	$B \rightarrow \mu \bar{e}$ 0.01 0.11	V_{bu} 0.002 0.08	$B \rightarrow \mu \bar{e}$ 0.005 0.08	*	V_{bu} 0.002 0.08
(21)	$D \rightarrow \mu \bar{e}$ 0.14 0.17	$K \rightarrow \mu \bar{e}$ 10^{-6} 0.12	$K \rightarrow \mu \bar{e}$ 10^{-6} 0.17	$K \rightarrow \mu \bar{e}$ 6×10^{-7} 0.07	$K \rightarrow \mu \bar{e}$ 6×10^{-7} 0.07	$D \rightarrow \mu \bar{e}$ 0.07 0.06	$K \rightarrow \mu \bar{e}$ 6×10^{-7} 0.03
(22)	$\mu \rightarrow e \gamma$ 5×10^{-5} 0.24	$\mu \rightarrow e \gamma$ 5×10^{-5} 0.16	0.20	$\mu \rightarrow e \gamma$ 0.07 0.10	$\mu \rightarrow e \gamma$ 0.07 0.10	$\mu \rightarrow e \gamma$ 9×10^{-3} 0.13	$\mu \rightarrow e \gamma$ 5×10^{-3} 0.05
(23)	*	$B \rightarrow \bar{\mu} e K$ 6×10^{-3} 0.21	$B \rightarrow \bar{\mu} e K$ 6×10^{-3} 0.21	$B \rightarrow \bar{\mu} e K$ 3×10^{-3} 0.13	$B \rightarrow \bar{\mu} e K$ 3×10^{-3} 0.13	*	$B \rightarrow \bar{\mu} e K$ 3×10^{-3} 0.13
(31)	*	$B \rightarrow \mu \bar{e}$ 0.01 0.20	$B \rightarrow \mu \bar{e}$ 0.01 0.20	V_{bu} 0.002 0.07	$B \rightarrow \mu \bar{e}$ 0.005 0.07	*	V_{bu} 0.002 0.07
(32)	*	$B \rightarrow \bar{\mu} e K$ 6×10^{-3} 0.26	$B \rightarrow \bar{\mu} e K$ 6×10^{-3} 0.26	$B \rightarrow \bar{\mu} e K$ 3×10^{-3} 0.11	$B \rightarrow \bar{\mu} e K$ 3×10^{-3} 0.11	*	$B \rightarrow \bar{\mu} e K$ 3×10^{-3} 0.11
(33)	*	0.29	0.29	$\mu \rightarrow e \gamma$ 0.001 0.15	$\mu \rightarrow e \gamma$ 0.001 0.15	*	$\mu \rightarrow e \gamma$ 0.001 0.15

5.2 High-mass leptoquark limits ($M_{LQ} \gg 300 \text{ GeV}$)

For high-mass leptoquarks, the cross section is proportional to the square of $\Psi_{eq_1 q_2} \equiv \lambda_{eq_1} \lambda_{\ell q_2} / M_{LQ}^2$, and a factor which does not depend on either the leptoquark couplings or mass (see equations 3 and 4). This is also true of rates for lower energy forbidden processes [10]. For a given limit on $\Psi_{eq_1 \ell q_2}$, the limit on the product $\lambda_{eq_1} \lambda_{\ell q_2}$ is proportional to M_{LQ}^2 . As M_{LQ} increases, the upper limit on the product of the couplings eventually exceeds unity and the perturbation expansion, on which the formulae in the appendix are based, breaks down. Even so, the parameter $\Psi_{eq_1 \ell q_2}$ serves as a reasonable figure of merit for experimental comparisons.

Tables 2, 3, 4 and 5 summarize the 95% CL upper bounds on $\Psi_{eq_1 \ell q_2}$, in units of 10^{-4} GeV^{-2} from this experiment and also from previous experiments [10]. Here q_1 and q_2 are the generation indices of the quarks which couple to e and to ℓ respectively¹². Two important characteristics of these tables are summarized below.

¹² Certain entries in these tables have been corrected and/or updated from reference [10] after consultation with the authors [38]

1. In the $e \leftrightarrow \mu$ case, for LQ species $V_{1/2}^L$, $\tilde{V}_{1/2}^L$, $S_{1/2}^L$, or $\tilde{S}_{1/2}^L$, the limits from this experiment supersede prior limits in some cases where heavy quark flavors are involved,
2. For the $e \leftrightarrow \tau$ case, we also improve upon existing limits for the same LQ species as in point 1. In addition, because the existing limits on $e \leftrightarrow \tau$ are much weaker than those for $e \leftrightarrow \mu$, the ZEUS limits are the most stringent for several additional LQs which couple to c or b quarks.

5.3 Limits for \mathcal{R}_P squarks

Coupling limits for S_0 and $\tilde{S}_{1/2}$ leptoquarks were converted to coupling limits on \tilde{d} , \tilde{u} , and \tilde{t} as described in Sect. 2.2. Figure 9 shows 95% CL limits on coupling vs. mass for \mathcal{R}_P squarks which decay to μq and τq . Here we assume the couplings at the production vertex (λ'_{11k} for \tilde{d}^k , λ'_{1j1} for \tilde{u}^j) and at the decay vertex (λ'_{ijk}) to be equal. The solid curves are the ZEUS limits which are given for two assumptions. The lower curves (and the \tilde{t} limits) assume that all squark decays are R -parity violating. The upper curves illustrate

Table 4. The best upper bounds on $\lambda_{eq_1}\lambda_{\tau q_2}/M_{LQ}^2$ for $F = 2$ leptoquarks, in units of 10^{-4} GeV^{-2} . Each column corresponds to a given leptoquark species and each row to the quark flavors q_1 and q_2 which couple to e and τ , the generation indices of which are specified in the first column. The top line in each box gives the previous measurement [10] which had obtained the strictest limit. The limit from that experiment is given on the second line in the box and the ZEUS limit, shown on the third line, is printed in boldface if it supersedes the previous limit. The asterisks denote those cases where lepton flavor violation occurs only via processes involving top

		$e \leftrightarrow \tau$			$F = 2$		
$(q_1 q_2)$	S_0^L	S_0^R	\tilde{S}_0^R	S_1^L	$V_{1/2}^L$	$V_{1/2}^R$	$\tilde{V}_{1/2}^L$
	$e^- u$	$e^- u$	$e^- d$	$e^-(u + \sqrt{2}d)$	$e^- d$	$e^-(u + d)$	$e^- u$
	νd			$\nu(\sqrt{2}u + d)$	νd		νu
(11)	G_F	$\tau \rightarrow \pi e$	$\tau \rightarrow \pi e$	G_F	$\tau \rightarrow \pi e$	$\tau \rightarrow \pi e$	$\tau \rightarrow \pi e$
	0.003	0.02	0.02	0.003	0.01	0.005	0.01
	0.15	0.15	0.23	0.09	0.09	0.05	0.06
(12)	$K \rightarrow \pi \bar{\nu} \nu$		$\tau \rightarrow K e$	$K \rightarrow \pi \bar{\nu} \nu$	$K \rightarrow \pi \bar{\nu} \nu$	$\tau \rightarrow K e$	
	2×10^{-5}		0.05	2×10^{-5}	10^{-5}	0.03	
	0.20	0.20	0.27	0.11	0.19	0.13	0.16
(13)	V_{bu}		$B \rightarrow \tau \bar{e} X$	V_{bu}	$B \rightarrow \tau \bar{e} X$	$B \rightarrow \tau \bar{e} X$	
	0.004		0.08	0.004	0.04	0.04	
		*	0.28	0.14	0.23	0.23	*
(21)	$K \rightarrow \pi \bar{\nu} \nu$		$\tau \rightarrow K e$	$K \rightarrow \pi \bar{\nu} \nu$	$K \rightarrow \pi \bar{\nu} \nu$	$\tau \rightarrow K e$	
	2×10^{-5}		0.05	2×10^{-5}	10^{-5}	0.03	
	0.22	0.22	0.31	0.12	0.09	0.05	0.06
(22)	$\tau \rightarrow e \gamma$	$\tau \rightarrow e \gamma$	$\tau \rightarrow e \gamma$	$\tau \rightarrow e \gamma$			
	0.5	0.5	0.3	0.1			
	0.60	0.60	0.48	0.22	0.25	0.19	0.31
(23)	$B \rightarrow \ell \nu X$		$B \rightarrow \tau \bar{e} X$	$B \rightarrow \ell \nu X$	$B \rightarrow \tau \bar{e} X$	$B \rightarrow \tau \bar{e} X$	
	0.04		0.08	0.04	0.04	0.04	
		*	0.50	0.25	0.33	0.33	*
(31)	$B \rightarrow \ell \nu X$		$B \rightarrow \tau \bar{e} X$	$B \rightarrow \ell \nu X$	$B \rightarrow \tau \bar{e} X$	$B \rightarrow \tau \bar{e} X$	
	0.04		0.08	0.04	0.04	0.04	
		*	0.34	0.17	0.10	0.10	*
(32)	$B \rightarrow \ell \nu X$		$B \rightarrow \tau \bar{e} X$	$B \rightarrow \ell \nu X$	$B \rightarrow \tau \bar{e} X$	$B \rightarrow \tau \bar{e} X$	
	0.04		0.08	0.04	0.04	0.04	
		*	0.65	0.32	0.26	0.26	*
(33)			$\tau \rightarrow e \gamma$	$\tau \rightarrow e \gamma$			
			0.3	0.1			
		*	0.72	0.36	0.38	0.38	*

the impact of gauge decays on the limits. They assume that a single R -parity conserving decay, namely $\tilde{q} \rightarrow q\tilde{\gamma}$ exists and that the photino is much lighter than the squark. Since our analysis is not sensitive to such decays (for which the branching fraction is given by equation 6) these limits are somewhat weaker. The stop mixing angle is assumed to be $\cos^2 \theta_t = 0.5$. The dashed curves are limits from low-energy experiments, adapted from reference [10]. Table 6 gives lower mass limits for \tilde{d} , \tilde{u} , and \tilde{t} assuming that the couplings at the production and decay vertices are equal to the electromagnetic coupling ($\sqrt{4\pi\alpha}$). As with the low-mass leptoquark case described earlier, the ZEUS limits improve on existing limits in cases where quark flavor change accompanies the lepton flavor change, especially for $e \leftrightarrow \tau$ flavor changes.

6 Conclusions

We have searched for signatures of lepton-flavor violation with the ZEUS detector. Hypothetical exotic particles such as leptoquarks could induce lepton-flavor violation observable at HERA. The tight constraints from sensitive searches

for processes such as muon conversion in titanium and rare muon and meson decays do not apply to all possible cases of LFV, many of which could be seen in ep collisions. Using 3.8 pb^{-1} of data taken at HERA during the 1993 and 1994 running periods, we have found no candidate events for LFV. The data permit us to constrain specific leptoquark coupling strengths as small as $10^{-3}\alpha$ and to exclude leptoquark masses as large as 270 GeV (for electromagnetic coupling) with 95% confidence. For $M_{LQ} \gg \sqrt{s}$, we calculate upper limits on the product of lepton flavor violating couplings divided by the square of the leptoquark mass, $\lambda_{eq_1}\lambda_{\ell q_2}/M_{LQ}^2$, and directly compare these with existing bounds from rare decays. Especially for $e \leftrightarrow \tau$ flavor changes, ZEUS has improved on existing limits for many flavor-violating scenarios.

Acknowledgements. We thank the HERA machine group for the excellent machine operation which made this work possible, the DESY computing and network group for providing the necessary data analysis environment, and the DESY directorate for strong support and encouragement. We wish to thank S. Davidson and H. Dreiner for useful discussions.

Table 5. The best upper bounds on $\lambda_{eq_1}\lambda_{\tau q_2}/M_{LQ}^2$ for $F = 0$ leptoquarks, in units of 10^{-4} GeV^{-2} . Each column corresponds to a given leptoquark species and each row to the quark flavors q_1 and q_2 which couple to e and τ , the generation indices of which are specified in the first column. The top line in each box gives the previous measurement [10] which had obtained the strictest limit. The limit from that experiment is given on the second line in the box and the ZEUS limit, shown on the third line, is printed in boldface if it supersedes the previous limit. The asterisks denote those cases where lepton flavor violation occurs only via processes involving top

		$e \leftrightarrow \tau$			$F = 0$		
$(q_1 q_2)$	$S_{1/2}^L$	$S_{1/2}^R$	$\tilde{S}_{1/2}^L$	V_0^L	V_0^R	\tilde{V}_0^R	V_1^L
	$e^- \bar{u}$	$e^- (\bar{u} + \bar{d})$	$e^- \bar{d}$	$e^- \bar{d}$	$e^- \bar{d}$	$e^- \bar{u}$	$e^- (\sqrt{2}\bar{u} + \bar{d})$
	$\nu \bar{u}$		$\nu \bar{d}$	$\nu \bar{u}$			$\nu (\bar{u} + \sqrt{2}\bar{d})$
(11)	$\tau \rightarrow \pi e$	$\tau \rightarrow \pi e$	$\tau \rightarrow \pi e$	G_F	$\tau \rightarrow \pi e$	$\tau \rightarrow \pi e$	G_F
	0.02	0.01	0.02	0.002	0.01	0.01	0.002
	0.11	0.09	0.18	0.11	0.11	0.07	0.04
(12)		$\tau \rightarrow Ke$	$K \rightarrow \pi \bar{\nu} \nu$	$\tau \rightarrow Ke$	$\tau \rightarrow Ke$		$K \rightarrow \pi \bar{\nu} \nu$
		0.05	2×10^{-5}	0.03	0.03		5×10^{-6}
	0.12	0.10	0.18	0.15	0.15	0.10	0.05
(13)		$B \rightarrow \tau \bar{e} X$	$B \rightarrow \tau \bar{e} X$	$B \rightarrow \ell \nu X$	$B \rightarrow \tau \bar{e} X$		$B \rightarrow \ell \nu X$
		0.08	0.08	0.02	0.04		0.02
	*	0.18	0.18	0.16	0.16	*	0.16
(21)		$\tau \rightarrow Ke$	$K \rightarrow \pi \bar{\nu} \nu$	$\tau \rightarrow Ke$	$\tau \rightarrow Ke$		$K \rightarrow \pi \bar{\nu} \nu$
		0.05	2×10^{-5}	0.03	0.03		5×10^{-6}
	0.34	0.26	0.39	0.14	0.14	0.10	0.05
(22)	$\tau \rightarrow e\gamma$	$\tau \rightarrow e\gamma$					
	0.2	0.2					
	0.60	0.37	0.48	0.25	0.25	0.31	0.13
(23)		$B \rightarrow \tau \bar{e} X$	$B \rightarrow \tau \bar{e} X$	$B \rightarrow \ell \nu X$	$B \rightarrow \tau \bar{e} X$		$B \rightarrow \ell \nu X$
		0.08	0.08	0.02	0.04		0.02
	*	0.50	0.50	0.33	0.33	*	0.33
(31)		$B \rightarrow \tau \bar{e} X$	$B \rightarrow \tau \bar{e} X$	V_{bu}	$B \rightarrow \tau \bar{e} X$		V_{bu}
		0.08	0.08	0.002	0.04		0.002
	*	0.47	0.47	0.15	0.15	*	0.15
(32)		$B \rightarrow \tau \bar{e} X$	$B \rightarrow \tau \bar{e} X$	$B \rightarrow \ell \nu X$	$B \rightarrow \tau \bar{e} X$		$B \rightarrow \ell \nu X$
		0.08	0.08	0.02	0.04		0.02
	*	0.65	0.65	0.26	0.26	*	0.26
(33)				$\tau \rightarrow e\gamma$	$\tau \rightarrow e\gamma$		
				3.4	3.4		
	*	0.72	0.72	0.38	0.38	*	0.38

Table 6. 95% CL mass limits (GeV) for squarks with \mathcal{R}_P -couplings, of electromagnetic strength ($\lambda_{11k}^2 = \lambda_{ijk}^2 = 4\pi\alpha = 4\pi/128$). The first line gives the mass limits for the case where the total branching fraction for gauge decays is 50%, the second line gives the mass limits for a squark which always has \mathcal{R}_P decays. The limits which assume 50% gauge decays are weaker because we did not search for the gauge decays. The mixing angle of the stop is assumed to be $\cos^2 \theta_t = 0.5$

	$\bar{d} \rightarrow \mu q$	$\bar{u} \rightarrow \mu q$	$\bar{t} \rightarrow \mu q$	$\bar{d} \rightarrow \tau q$	$\bar{u} \rightarrow \tau q$	$\bar{t} \rightarrow \tau q$
50% gauge decays	217	223	-	209	216	-
no gauge decays	231	234	223	223	228	216

Appendix

We summarize here the cross section formulae [9] for processes involving leptoquarks which couple only to left-handed or right-handed leptons. Process (1) can be mediated by either s -channel or u -channel leptoquark exchange. For the s -channel process, $e q_1 \rightarrow \ell q_2$, the differential cross section, for unpolarized beams, can be written as:

$$\frac{d^2\sigma}{dx dy} = \frac{1}{32\pi x s} q_1(x, \hat{s}) \frac{\lambda_{eq_1}^2 \lambda_{\ell q_2}^2 s^2 x^2}{(sx - M_{LQ}^2)^2 + M_{LQ}^2 \Gamma_{LQ}^2}$$

$$\times \begin{cases} \frac{1}{2} & \text{scalar } LQ \\ 2(1-y)^2 & \text{vector } LQ, \end{cases} \quad (7)$$

where $q_1(x, \hat{s})$ is the parton density¹³ for the initial state quark or antiquark, λ_{eq_1} and $\lambda_{\ell q_2}$ are the couplings at the production and decay vertices, and Γ_{LQ} is the total width of the leptoquark. The partial width for decay into lepton ℓ , and quark q_2 , is

¹³ For s - and u -channel processes, we have used \hat{s} and $-u$ respectively as the scale in the parton densities. If we had used Q^2 , the calculated cross sections would vary by less than 4% for initial-state u and d quarks and by less than 16% for initial-state s , c , or b quarks

$$\Gamma_{\ell q_2} = M_{LQ} \lambda_{\ell q_2}^2 \times \begin{cases} \frac{1}{16\pi} & \text{scalar } LQ \\ \frac{1}{24\pi} & \text{vector } LQ, \end{cases} \quad (8)$$

so that the typical LQ sought here has $\Gamma_{LQ} \ll M_{LQ}$. In the narrow width approximation, which holds when the variation of $q_1(x)$ is small as x is varied by $\delta x \sim \Gamma_{LQ}/M_{LQ}$, integration of equation (7) leads to the formula 2, with $B_{\ell q_2} = \Gamma_{\ell q_2}/\Gamma_{LQ}$.

For the u -channel process $e q_2 \rightarrow \ell q_1$, the differential cross section is given by:

$$\frac{d^2\sigma}{dx dy} = \frac{1}{32\pi x s} q_2(x, -u) \frac{\lambda_{e q_2}^2 \lambda_{\ell q_1}^2 s^2 x^2}{[s x (1-y) + M_{LQ}^2]^2} \times \begin{cases} \frac{1}{2} (1-y)^2 & \text{scalar } LQ \\ 2 & \text{vector } LQ. \end{cases} \quad (9)$$

In the limit that $M_{LQ}^2 \gg s$, integration of equations (7) and (9) lead to equations (3) and (4), which are accurate to better than 10% for $M_{LQ} > 500$ GeV.

Note that any leptoquark will take part in both s - and u -channel interactions. For example an S_0^R leptoquark will mediate the s -channel process $e^+ \bar{u} \rightarrow \mu^+ \bar{c}$ as well as the u -channel reaction $e^+ c \rightarrow \mu^+ u$.

References

1. S. Ahmad et al., Phys. Rev. **D38** (1988) 2102 ;
T. Kosmas et al., Nucl. Phys. **A570** (1994) 637.
2. A. van der Schaff, Progress in particle and nuclear physics, **31** (1993) 1.
3. L.M. Sehgal, PITHA-94-52 (1994) 1.
4. H. Kroha, Mod. Phys. Lett. **A8** (1993) 869.
5. I.I. Bigi, G. Köpp, and P.M. Zerwas, Phys. Lett. **166B** (1986) 238.
6. S. Yang, Ph.D. thesis, Columbia University, CU-95-396 (1995).
7. H1 Coll., S. Aid et al., Phys. Lett **369B** (1996) 173.
8. B. Schrempp, Proc. of the 1991 Workshop on Physics at HERA, ed. W. Buchmüller and G. Ingelman, (DESY, Hamburg 1992), p.1034, and references therein.
9. W. Buchmüller, R. Rückl, and D. Wyler, Phys. Lett. **191B** (1987) 442.
10. S. Davidson, D. Bailey, and B. Campbell, Z. Phys. **C61** (1994) 613.
11. L3 Coll., B. Adeva et al., Phys. Lett. **261B** (1991) 169;
OPAL Coll., G. Alexander et al., Phys. Lett. **263B** (1991) 123;
DELPHI Coll., P. Abreu et al., Phys. Lett. **316B** (1993) 620.
12. CDF Coll., F. Abe et al., Phys. Rev. Lett. **75** (1995) 1012;
D0 Coll., S. Abachi et al., Phys. Rev. Lett. **75** (1995) 3618.

13. V. Barger, G.F. Giudice, and T. Han, Phys. Rev. **D40** (1989) 2987.
14. J. Butterworth and H. Dreiner, Nucl. Phys. **B397** (1993) 3, and references therein.
15. T. Kon and T. Kobayashi, Phys. Lett. **B270** (1991) 81;
T. Kon, T. Kobayashi and K. Nakamura, Proc. of the 1991 Workshop on Physics at HERA, ed. W. Buchmüller and G. Ingelman, (DESY, Hamburg 1992), p.1088.
16. The ZEUS Detector, Status Report 1993, DESY 1993.
17. M. Derrick et al., Nucl. Inst. Meth. **A309** (1991) 77;
A. Andresen et al., Nucl. Inst. Meth. **A309** (1991) 101;
A. Bernstein et al., Nucl. Inst. Meth. **A336** (1993) 23;
A. Caldwell et al., Nucl. Inst. Meth. **A321** (1992) 356.
18. N.Harnew et al., Nucl. Inst. Meth. **A279**(1989)290;
B.Foster et al., Nucl. Phys., Proc. Suppl. **B32**(1993);
B.Foster et al., Nucl. Inst. Meth. **A338**(1994)254
19. G. Abbiendi et al., Nucl. Inst. Meth. **A333** (1993) 342.
20. J. Andruszków et al., DESY 92-066 (1992).
21. PYTHIA 5.6 and JETSET 7.4, H.U. Bengtsson, T. Sjöstrand, Comp. Phys. Comm. **46** (1987) 43.
22. LEPTO 6.1, G. Ingelman, Proc. of the 1991 Workshop on Physics at HERA, ed. W. Buchmüller and G. Ingelman, (DESY, Hamburg 1992), p.1366.
23. HERACLES 4.1, A. Kwiatkowski, H. Spiesberger and H.J. Möhring, Proc. of the 1991 Workshop on Physics at HERA, ed. W. Buchmüller and G. Ingelman, (DESY, Hamburg 1992), p.1294.
24. DJANGO 6.1, G. Schuler et al., Proc. of the 1991 Workshop on Physics at HERA, ed. W. Buchmüller and G. Ingelman, (DESY, Hamburg 1992), p.1419.
25. A.D. Martin, W.J. Stirling, and R.G. Roberts, Phys. Rev. **D50** (1994) 6734.
26. ARIADNE 4.03, L. Lönnblad, LU TP-89-10 (1989);
L. Lönnblad, Comp. Phys. Comm. **71** (1992) 15.
27. HERWIG 5.8, G. Marchesini et al., Comp. Phys. Comm. **67** (1992) 465.
28. AROMA 2.1, G. Ingelman and G. Schuler, Proc. of the 1991 Workshop on Physics at HERA, ed. W. Buchmüller and G. Ingelman, (DESY, Hamburg 1992), p.1346.
29. A generator based on J.A.M. Vermaseren, Nucl. Phys. **B229** (1983) 347.
30. U. Baur, J.A.M. Vermaseren, and D. Zeppenfeld, Nucl. Phys. **B375** (1992) 3.
31. R. Brun et al., CERN DD/EE-84-1 (1987).
32. L. Montanet et al., Review of Particle Properties, Phys. Rev. **D50** (1994) 1173 (see p. 1281).
33. M. Glück, E. Reya, and Vogt, Z. Phys. **C53** (1992) 127.
34. A.D. Martin, W.J. Stirling, R.G. Roberts, RAL-93-077 (1993).
35. Crystal Ball Coll., S. Keh et al., Phys. Lett. **B212** (1988) 123.
36. K.G. Hayes et al., Phys. Rev. **D25** (1982) 2869.
37. CLEO Coll., R. Ammar et al., Phys. Rev. **D49** (1994) 5701.
38. Private communications with S. Davidson.